

GWT: Scalable Optimizer State Compression for Large Language Model Training

Ziqing Wen, Ping Luo, Jiahuan Wang, Kun Yuan, *Member, IEEE*, Dongsheng Li, and Tao Sun

Abstract—Large Language Models (LLMs) have demonstrated exceptional capabilities across diverse natural language processing benchmarks. However, the escalating scale of model parameters imposes prohibitive memory overheads during training, especially when employing stateful optimizers such as Adam. Conventional memory-efficient strategies, typically involving singular value decomposition (SVD) or weight freezing, often incur non-negligible performance degradation relative to full-rank updates. To address these limitations, this paper explores memory-efficient optimization beyond low-rank constraints and proposes the Gradient Wavelet Transform (GWT). GWT characterizes a novel compression framework that projects gradients into wavelet subspaces, effectively compacting optimizer states while preserving essential update information. We theoretically and empirically demonstrate that GWT can be seamlessly integrated into existing optimization protocols, facilitating resource-efficient training without compromising model fidelity. Rigorous evaluations encompassing both large-scale pre-training and task-specific fine-tuning reveal that GWT yields performance parity with advanced memory-efficient optimizers and full-rank updates. Furthermore, GWT provides a scalable and robust solution for managing the memory-intensive pipelines inherent in modern large-scale data engineering and knowledge discovery systems.

Index Terms—Memory-efficient training, Wavelet transform, Optimization, Large language models.

I. INTRODUCTION

LARGE Language Models (LLMs) have made remarkable strides since the release of ChatGPT [1]. Their promising performance and scalability have led to rapid adoption across a range of fields [2]–[5]. The impressive capabilities of LLMs arise from their vast number of parameters and the massive datasets used for training. However, training these models imposes significant demands on the optimizer, with Adam [6] emerging as the most commonly used optimizer due to its fast convergence, robustness, and considerable experimental results.

Despite these advantages, Adam’s memory requirements present a major drawback. Specifically, it consumes twice the memory of the model itself (as illustrated in Figure 1), making memory usage a key bottleneck in LLM training. For instance, pre-training a LLaMA 7B [4] model requires approximately 58GB of GPU memory: 14GB for model weights, 14GB for gradients, 2GB for activations, and 28GB for Adam optimizer

states under BF16 precision [7]. When the model size exceeds 100B parameters, such as GPT-3 (175B parameters) [1], the additional memory overhead from Adam may exceed 700GB, requiring at least 9 additional NVIDIA A100 80GB GPUs.

Given the high costs of training LLMs, methods that reduce the batch size or use larger GPUs quickly become unsustainable. To mitigate these issues, many studies have focused on optimizing memory usage in LLM training. A promising solution is low-rank training [7], [8], which has made significant progress in alleviating memory constraints. These memory-efficient methods can be broadly classified into two categories: weight-based and gradient-based approaches [9]. Notable examples include Low-Rank Adaptation (LoRA) [8] and Gradient Low-Rank Projection (GaLore) [7].

LoRA leverages the low-rank nature of model parameter updates by freezing the pre-trained model weights and reparameterizing weight updates with trainable low-rank decomposition matrices. Extensive experiments have demonstrated that LoRA is effective in fine-tuning tasks, but its performance in pre-training remains limited. Additionally, the strong low-rank assumptions underlying LoRA often result in suboptimal outcomes [10], [11]. FLoRA [12], on the other hand, uses resampling projection matrices to address the low-rank constraints of LoRA.

In contrast to LoRA, which decomposes the update matrix, GaLore reduces the optimizer state memory usage by performing Singular Value Decomposition (SVD) on the gradients, since the memory occupied by optimizer states is directly tied to the gradient size (as shown in Figure 1). GaLore has demonstrated effective performance in both pre-training and fine-tuning tasks. However, its performance still lags behind that of full-rank methods, and it only captures information within the projected subspace, discarding gradient information outside of it. This limitation becomes particularly problematic when using lower ranks or when gradients are noisy [9], [13].

To address these challenges, Fira [9] introduces the error residual between the full-rank gradient and its subspace projection, while GoLore [13] enhances GaLore by utilizing random projection to better capture gradient information when noise is dominant. However, these methods still rely on SVD for updating the subspace, and the high computational cost of SVD ($O(m^2 \times n)$ for a matrix of size $m \times n$) can significantly slow down training, particularly for large models. To mitigate this issue, APOLLO [14] proposes an SVD-free variant of GaLore, replacing SVD with random projections. This modification not only improves training speed but also leads to enhanced empirical performance.

While it is intuitive to expect that information loss in low-

Corresponding author: Tao Sun.

Ziqing Wen, Ping Luo, Jiahuan Wang, Dongsheng Li, Tao Sun are with the National Key Laboratory of Parallel and Distributed Computing, National University of Defense Technology, Changsha, 410073, China (e-mail: zqw@nudt.edu.cn; luoping@nudt.edu.cn; wangjiahuan@nudt.edu.cn; dsli@nudt.edu.cn); suntao.saltfish@outlook.com.

Kun Yuan is with Center for Machine Learning Research, Peking University, Beijing 100871, China (e-mail: kunyuan@pku.edu.cn).

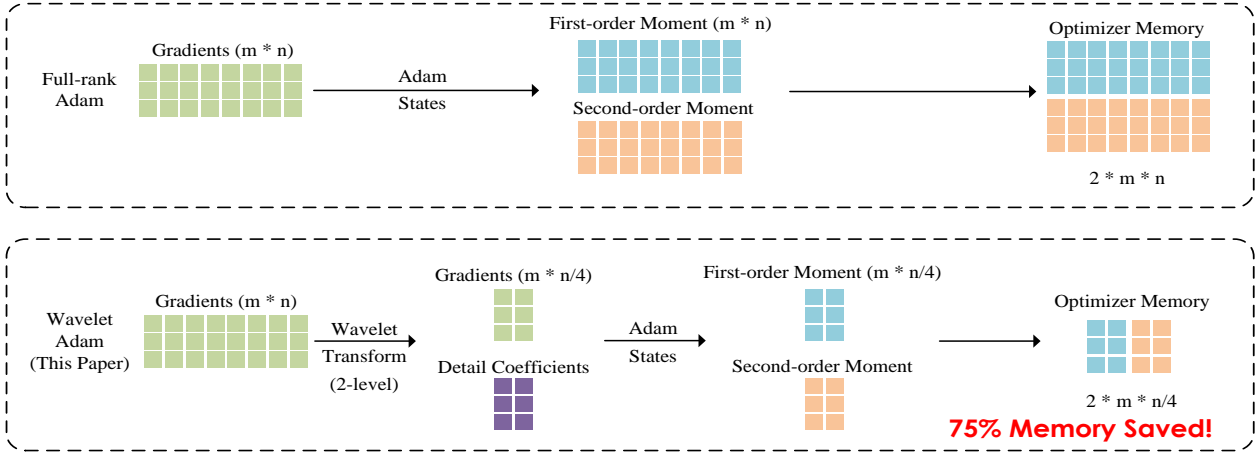


Fig. 1. **Visualization of memory usage for Adam optimizer states.** Compared with full-rank Adam, the 2-level wavelet transform can reduce the optimizer state by up to 75%.

rank approximations would degrade performance relative to full-rank training, extensive experiments have shown otherwise: both Fira and APOLLO have **surprisingly outperformed full-rank training** in various settings. These findings underscore the potential of memory-efficient optimization algorithms as strong alternatives to full-rank methods, making efficient training not only necessary but also beneficial in practice.

The above methods are based on low-rank decomposition. Aside from low-rank decomposition, the Wavelet Transform (WT) also has wide applications in the field of compression. Compared with low-rank decomposition, wavelet transform has lower computational complexity ($O(m \times n)$), better captures local information features, and suppresses high-frequency noise [15]. Moreover, due to its robustness to noise, it is better suited for stochastic gradient descent, a training method that involves noise. Therefore, we can naturally raise the following question:

Can wavelet decomposition, like SVD, benefit the training of large language models, reducing memory consumption and improving model performance?

To address the limitations of existing low-rank training methods, we introduce the Gradient Wavelet Transform (GWT), a simple yet effective plug-and-play framework that applies wavelet transforms to gradients during training. By leveraging the natural sparsity and localization properties of wavelets, GWT compresses gradient representations and significantly reduces the memory required to store optimizer states without relying on low-rank assumptions. Distinct from traditional matrix-based compression techniques, GWT is the first method to adopt a frequency-domain perspective for gradient compression. It achieves memory efficiency by selectively controlling low- and high-frequency coefficients. When applied to large-scale language model pretraining, such as LLaMA on the C4 dataset, GWT achieves up to 79%

optimizer memory reduction and 1.9× training speedup on 3B models, all while maintaining or even improving model quality. Moreover, GWT integrates seamlessly with optimizers beyond Adam, highlighting its versatility across different training regimes. These results demonstrate that GWT provides a **practical, optimizer-agnostic, and highly efficient solution** for memory-constrained deep learning.

II. RELATED WORKS

TABLE I
MEMORY AND COMPLEXITY COMPARISON OF DIFFERENT METHODS. SUPPOSE $W \in \mathbb{R}^{m \times n}$ ($m \leq n$), GALORE AND LORA ADOPT A RANK OF r , GWT APPLIES A LEVEL OF l .

	Full-Adam	GaLore	APOLLO	LoRA	GWT
Weights	mn	mn	mn	$mn + mr + nr$	mn
Optimizer States	$2mn$	$mr + 2nr$	$mr + 2nr$	$2mr + 2nr$	$mn/2^{l-1}$
Complexity	$\mathcal{O}(mn)$	$\mathcal{O}(mn^2)$	$\mathcal{O}(mnr)$	$\mathcal{O}(mn + mr + nr)$	$\mathcal{O}(mnl)$

Memory-Efficient Optimizers. Given the high memory requirements of the Adam optimizer [6], numerous approaches aim to improve the optimizer or create new optimization methods to reduce training costs for LLMs. Low-Rank Adaptation (LoRA) [8], which addresses this issue by freezing the parameters of the pre-trained model and introducing trainable low-rank matrices that decompose the pre-trained weights. LoRA has proven to be an effective strategy for optimizing the training of large language models, and several subsequent studies have built upon this framework to further enhance optimization performance [10]–[12], [16], [17]. Gradient Low-Rank Projection (GaLore) [7] lowers the memory cost of optimizer states by projecting gradients into a lower-dimensional subspace. This method not only facilitates full-parameter LLM training but also delivers strong performance in both pretraining and fine-tuning tasks. Recent GaLore-based extensions have shown experimental results that outperform full-rank methods [9], [14], [18]. More recently, MUON [19] achieves adaptive learning rates by leveraging only momentum

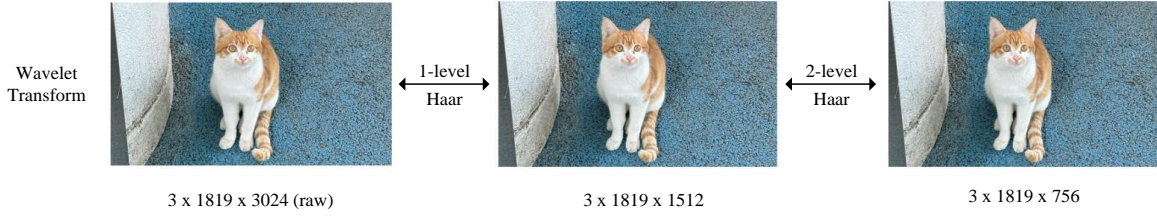


Fig. 2. **Visualization of the approximation coefficients of a 2-Level DHT on an image (rescaled for visual clarity).** Even after reducing the image to 25% of its original size (right), the approximation coefficients successfully preserve the key structural features of the image.

and matrix orthogonalization. Additionally, methods based on gradient normalization, such as SWAN [20], SinkGD [21], and SCALE [22] enable SGD-style updates that further reduce memory overhead.

System Memory Efficiency. Beyond optimizing memory usage at the level of the optimizer, some strategies target reducing memory consumption in the overall system. Gradient checkpointing [23] is one such method that conserves memory by not storing activation values. Quantization techniques [24], [25] further reduce memory overhead by employing lower-bit data representations. These methods have significantly accelerated and optimized LLM training processes. Our GWT approach offers a distinct advantage over these techniques by providing a memory-efficient alternative. Moreover, our method is designed to be compatible with existing system-level optimization strategies, allowing for a synergistic integration that can lead to even faster and more efficient LLM training.

III. METHODS

In this section, we first provide an overview of the fundamental theory behind wavelet transforms, followed by a detailed explanation of how the proposed Gradient Wavelet Transform (GWT) method is integrated into the Adam optimizer [6] and a theoretical analysis of the relationship between wavelet transform and low-rank approximation.

A. Discrete Haar Wavelet Transform

Wavelet transforms can be categorized into continuous and discrete types. In this paper, we mainly focus on the discrete Haar wavelet due to its simple and easy-to-understand basis functions, high computational efficiency, broad applicability to compression tasks [26], and the fact that the total amount of data after decomposition equals the original data, without introducing extra information. It decomposes a signal (or image) into two main components: (a) Approximation coefficients (low-frequency), which represent the smooth or average part of the signal/image, and (b) Detail coefficients (high-frequency), which capture the finer details or differences in the signal/image.

For example, for an input signal or image represented by the sequence of values $[x_1, x_2, x_3, x_4, x_5, x_6, x_7, x_8]$, the 1-

level Discrete Haar Transform (DHT, Haar-1) computes the Approximation and Detail coefficients as follows

$$A_1 = \left[\frac{x_1 + x_2}{\sqrt{2}}, \frac{x_3 + x_4}{\sqrt{2}}, \frac{x_5 + x_6}{\sqrt{2}}, \frac{x_7 + x_8}{\sqrt{2}} \right],$$

$$D_1 = \left[\frac{x_1 - x_2}{\sqrt{2}}, \frac{x_3 - x_4}{\sqrt{2}}, \frac{x_5 - x_6}{\sqrt{2}}, \frac{x_7 - x_8}{\sqrt{2}} \right].$$

The wavelet filter for DHT is $[\frac{1}{\sqrt{2}}, \frac{1}{\sqrt{2}}]$ for approximation, and $[\frac{1}{\sqrt{2}}, -\frac{1}{\sqrt{2}}]$ for detail coefficients. The reconstruction of the original signal can be expressed as follows

$$[x_1, x_3, x_5, x_7] = \frac{A_1 + D_1}{\sqrt{2}}, [x_2, x_4, x_6, x_8] = \frac{A_1 - D_1}{\sqrt{2}}. \quad (1)$$

Next, we can apply an additional DHT transform to the approximation coefficient A_1 , yielding the following results:

$$A_2 = \left[\frac{x_1 + x_2 + x_3 + x_4}{2}, \frac{x_5 + x_6 + x_7 + x_8}{2} \right],$$

$$D_2 = \left[\frac{x_1 + x_2 - x_3 - x_4}{2}, \frac{x_5 + x_6 - x_7 - x_8}{2} \right].$$

Therefore, we have derived a simple implementation of 2-level DHT, the corresponding reconstruction is similar to 1-level. The DHT converts a vector with eight elements into two vectors (A_1, D_1) of 4 elements each or three vectors (A_2, D_2, D_1). Storing just approximation coefficients will reduce our memory cost by 50% or 75%. This process can be repeated iteratively, breaking the signal into increasingly finer levels of approximation and detail, facilitating efficient compression and storage.

Building on the derivation above, we can represent the Discrete DHT as a matrix projection. For a more general formulation, let $W \in \mathbb{R}^{m \times n}$ be a matrix (we suppose $n \bmod 2 = 0$ for simplicity). The DHT and reconstruction can be expressed as:

$$[A, D] = WH, \quad W = [A, D]H^T, \quad (2)$$

where $A, D \in \mathbb{R}^{m \times \frac{n}{2}}$, $H \in \mathbb{R}^{n \times n}$ denote the Haar wavelet transform matrix, and the elements are defined as:

$$H_{2i-1, i} = H_{2i, i} = H_{2i-1, \frac{n}{2}+i} = \frac{1}{\sqrt{2}}, H_{2i, \frac{n}{2}+i} = -\frac{1}{\sqrt{2}} \quad (3)$$

It is straightforward that $HH^T = I$, where I is the identity matrix. For higher-level DHT, the formulation is similar. This matrix-based representation allows for efficient computation and generalization of the DHT to higher-dimensional cases,

Algorithm 1 Adam with Wavelet Transform

Input: Weight matrix W , step size η , batch size m , decay rates β_1, β_2 , iteration T , ϵ for numerical stability, scale factor α , wavelet transform level l , and wavelet transformer H^l .

Initialize $t \leftarrow 0$

repeat

$G_t \leftarrow \frac{1}{m} \sum_{i=1}^m \nabla_W f_i(W_t)$ {Batch gradient}
 $[A_t, D_t] \leftarrow G_t H^l$ {Gradient wavelet transform}

if $t = 0$ **then**

Initialize $M_{-1}, V_{-1} \leftarrow 0$

end if

Adam states update

$M_t^R \leftarrow \beta_1 \cdot M_{t-1}^R + (1 - \beta_1) \cdot A_t$
 $V_t^R \leftarrow \beta_2 \cdot V_{t-1}^R + (1 - \beta_2) \cdot A_t^2$
 $[\tilde{A}_t, \tilde{D}_t] \leftarrow [M_t^R / (\sqrt{V_t^R} + \epsilon), D_t / (\sqrt{V_t^R} + \epsilon)]$

$\tilde{G}_t \leftarrow \alpha \cdot [\tilde{A}_t, \tilde{D}_t] H^T$ {Wavelet transform back}

$\eta_t \leftarrow \eta \cdot \frac{\sqrt{1 - \beta_2^t}}{(1 - \beta_1^t)}$ {Bias correction}

$W_t \leftarrow W_{t-1} - \eta_t \cdot \tilde{G}_t$ {Update weights}

$t \leftarrow t + 1$

until $t = T$

return W_t

making it a powerful tool for applications such as gradient compression in optimization methods.

B. Adam with GWT

The Adam optimizer [6] adaptively adjusts the learning rates for each parameter based on its past gradient states, while also incorporating momentum to accelerate training. The update rule for the weights is given by the following recursive equation:

$$W_{t+1} = W_t - \eta \cdot \tilde{G}_t, \tilde{G}_t = \frac{M_t}{\sqrt{V_t} + \epsilon} \quad (4)$$

where $\eta > 0$ denotes the learning rate, \cdot represents the element-wise multiplication, $W \in \mathbb{R}^{m \times n}$ and

$$\begin{aligned} M_t &= \beta_1 \cdot M_{t-1} + (1 - \beta_1) \cdot G_t, \\ V_t &= \beta_2 \cdot V_{t-1} + (1 - \beta_2) \cdot G_t^2. \end{aligned} \quad (5)$$

Here, $\beta_1, \beta_2 \in [0, 1)$ are the decay rates hyperparameters which are set as 0.9, 0.999 commonly, $\epsilon > 0$ to preserve numerical stability, $G_t \in \mathbb{R}^{m \times n}$ denotes the batch gradient at time step t , and $M, V \in \mathbb{R}^{m \times n}$ represents the first/second-order moment in Adam optimizer.

For ease of presentation, we adopt a 1-level DHT in the following discussion. To integrate GWT with the Adam optimizer, we begin by applying GWT to the gradient matrix G_t at time step t (Eq. (2)), focusing on the approximate coefficients. This results in a compressed gradient matrix (approximation coefficient) $A_t \in \mathbb{R}^{m \times \frac{n}{2}}$ and a detail coefficient matrix $D_t \in \mathbb{R}^{m \times \frac{n}{2}}$. We then update the Adam states by replacing the original gradient G_t in the update rule (Eq. (5)) with the

smaller matrix A_t to calculate \tilde{G}_t . To preserve the consistency of the state update, we scale the wavelet detail coefficients D_t by dividing them by $\sqrt{V_t^R} + \epsilon$ based on the linear properties of DHT (Eq. (2)). Finally, project \tilde{G}_t back to the original space and update the weights. The update rule can be rewritten as follows if we have $[A_t, D_t] = G_t H$,

$$M_t^R = \beta_1 \cdot M_{t-1}^R + (1 - \beta_1) A_t, V_t^R = \beta_2 V_{t-1}^R + (1 - \beta_2) A_t^2. \quad (6)$$

Then, compute the normalized coefficients by

$$\tilde{A}_t = \frac{M_t^R}{\sqrt{V_t^R} + \epsilon}, \tilde{D}_t = \frac{D_t}{\sqrt{V_t^R} + \epsilon}.$$

Owing to the linear transformation property of the wavelet transform, we divide the detail coefficients D_t by $\sqrt{V_t^R}$ to maintain scale consistency. Therefore, we can update the weight in the original space

$$\tilde{G}_t = [\tilde{A}_t, \tilde{D}_t] H^T, W_{t+1} = W_t - \eta_t \cdot \tilde{G}_t$$

The procedure for applying GWT to the Adam optimizer is outlined in Algorithm 1. We implement the Adam optimizer with Haar-2 on the LLaMA 130M model, and present the learning curve in Figure 3. We observe that the learning curve (blue) demonstrates a twice spike around the 900th and 2500th iteration. This phenomenon is likely due to unstable gradients during the early stages of training, as observed in previous studies [9], [27]. To address this issue, we adopt the Norm-growth Limiter (NL) technique introduced by Fira [9], which stabilizes gradient growth. NL controls the ratio of the current gradient norm to the previous gradient norm by rescaling the current gradient as follows

$$\text{if } \frac{\|\tilde{G}_t\|_F}{\|\tilde{G}_{t-1}\|_F} > \gamma \text{ then } \tilde{G}_t \leftarrow \frac{\tilde{G}_t}{\|\tilde{G}_t\|_F} \cdot \gamma \cdot \|\tilde{G}_{t-1}\|_F,$$

where γ is a threshold that limits the gradient norm growth, we adopt $\gamma = 1.01$ by default. This technique significantly reduces the impact of unstable gradients in the early training stages [14]. After introducing NL, the learning curve (orange) for our Haar-2 implementation becomes smoother, resulting in a lower training loss.

In summary, we integrate the proposed GWT method into the Adam optimizer and observe that it can theoretically reduce the memory footprint of optimizer states by up to 75%. GWT achieves this by projecting gradients into a lower-dimensional subspace and performing updates to the optimizer states within this subspace. This memory-efficient strategy significantly reduces the storage requirements and can be applied to a wide range of optimizers that maintain substantial state information.

Importantly, the GWT is not limited to Adam. We provide the empirical results demonstrating that GWT, when integrated with optimizers such as Adam-mini [28] and MUON [19], achieves comparable performance to those optimizers.

C. Theoretical Analysis

In this section, we analyze how the gradient matrix arising from training over-parameterized models can be efficiently

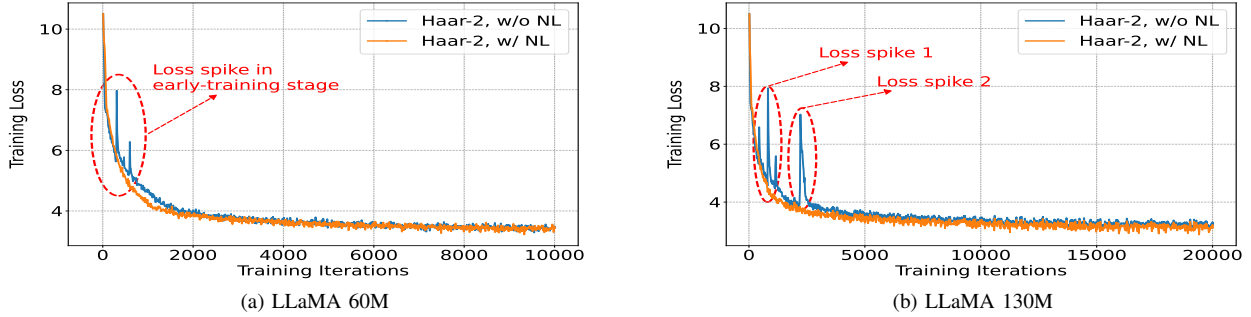


Fig. 3. Training loss comparison between Haar-2 with/without NL on LLaMA 60M and 130M.

approximated using Haar wavelet low-pass operators. We show that, under mild sequential smoothness assumptions, block-wise averaging over the columns yields a low-rank-like approximation that can outperform traditional global rank- r approximations in Frobenius norm.

Fix a level $l \geq 0$ and let the block length be $b = 2^l$ dividing n . Partition the columns of $G \in \mathbb{R}^{m \times n}$ into consecutive blocks

$$\mathcal{B}_k := \{(k-1)b + 1, \dots, kb\}, \quad k = 1, \dots, q, \quad q = n/b.$$

The Haar low-pass operator $P_l : \mathbb{R}^{m \times n} \rightarrow \mathbb{R}^{m \times n}$ replaces each column in a block with the block mean

$$(P_l(G))_{:,j} := \bar{g}_k, \quad j \in \mathcal{B}_k, \quad \bar{g}_k := \frac{1}{b} \sum_{t \in \mathcal{B}_k} G_{:,t} \in \mathbb{R}^m.$$

As a result, $P_l(G)$ has the same dimension as G , but all columns in the same block are identical, effectively removing high-frequency variation within the block.

To formalize the effectiveness of this approximation, we impose a sequential smoothness assumption on G . Let $\Delta : \mathbb{R}^{m \times n} \rightarrow \mathbb{R}^{m \times (n-1)}$ denote the column difference operator

$$(\Delta G)_{:,j} := G_{:,j+1} - G_{:,j}, \quad j = 1, \dots, n-1.$$

Assumption 1 (Column Smoothness). For some integer $r \geq 0$, the gradient matrix satisfies

$$\|\Delta G\|_F < [\sin(\pi/b)\sqrt{r}] \sigma_{r+1}(G),$$

where $\sigma_{r+1}(G)$ is the $(r+1)$ -th singular value of G .

Under this assumption, the following theorem establishes that the Haar low-pass approximation $P_l(G)$ can outperform any global rank- r approximation in Frobenius norm.

Theorem 1 (Haar Low-Pass Dominance). *Under Assumption 1, the Haar level- l low-pass approximation $P_l(G)$ satisfies*

$$\|G - P_l(G)\|_F < \inf_{\text{rank}(X) \leq r} \|G - X\|_F.$$

In practice, for LLM training with $m \approx n$, $r \sim n/4$, and $l = 3$, the smoothness condition reduces to

$$\|\Delta G\|_F < 0.1913\sqrt{n} \sigma_{r+1}(G),$$

which is typically satisfied due to sequential correlations in the data. Intuitively, the Haar averaging preserves the low-frequency structure of the gradient matrix while discarding

small within-block fluctuations that a low-rank approximation might not capture. Detailed proofs and eigenvalue-based bounds are provided in Appendix.

IV. EXPERIMENTS

In this section, we demonstrate that the Gradient Wavelet Transform (GWT), as a memory-efficient optimization technique, can achieve performance comparable to or even surpassing that of full-rank optimizers, while significantly reducing memory usage and increasing training throughput. Specifically, we evaluate GWT in two contexts: pre-training LLaMA [29] models on the Colossal Clean Crawled Corpus (C4) [30] English benchmark, fine-tuning various pre-trained models on the Multi-task Language Understanding (MMLU) [31] and RoBERTa-base on the General Language Understanding Evaluation (GLUE) [32] benchmarks. We adopt the BF-16 format to reduce memory usage across all experiments and provide a detailed description of these datasets in the Appendix.

For GWT, we use the discrete Haar wavelet as the default filter. Additionally, we present an ablation study to examine the impact of key hyperparameters, including the scale factor (α), initial learning rate (lr), the GWT level (l), and generalization to models beyond LLaMA. A comprehensive description of the experimental setup can be found in the Appendix.

A. Memory-efficient Pre-Training

We integrate our proposed GWT method into the Adam optimizer [6], using default hyperparameters ($\beta_1 = 0.9$, $\beta_2 = 0.999$, $\epsilon = 10^{-6}$), and evaluate its performance on the LLaMA models using the C4 pretraining task. To provide a comprehensive comparison, we include our reproduced results for full-rank Adam [6], GaLore [7], and APOLLO [14], alongside reference results reported by Fira [9], and LoRA [7]. All experiments adopt a consistent configuration: we use GaLore’s default hyperparameters ($lr = 0.01$, $\alpha = 0.25$) for both GaLore and GWT, and $\alpha = 1.0$ for APOLLO. A cosine annealing schedule is applied to the learning rate. We use a sequence length of 256 and a batch size of 512, resulting in a total of 131K tokens per batch, unless stated otherwise.

For GaLore-r and APOLLO-r, we experiment with compression ratios corresponding to one-fourth and one-eighth of the model rank, referred to as GaLore-1/4 and GaLore-1/8, respectively. These settings are consistent with GWT

TABLE II
FINAL VALIDATION PPL (LOWER IS BETTER) AND ESTIMATED MEMORY USAGE ON PRE-TRAINING LLaMA MODELS ON THE C4 DATASET.
RESULTS MARKED WITH * INDICATE VALUES REPORTED IN PREVIOUS WORKS.

Methods	60M	130M	350M	1B
Full-Rank Adam	33.37 (0.34G)	25.08 (0.80G)	18.75 (2.20G)	16.10 (8.03G)
MUON	28.93 (0.30G)	23.05 (0.63G)	16.96 (1.60G)	14.28 (5.61G)
GaLore-1/4	39.94 (0.28G)	26.47 (0.58G)	19.36 (1.38G)	15.66 (4.76G)
APOLLO-1/4	31.53 (0.28G)	23.35 (0.58G)	16.73 (1.38G)	14.10 (4.76G)
GWT-2	29.35 (0.27G)	22.47 (0.55G)	16.29 (1.24G)	13.50 (4.41G)
GaLore-1/8	48.48 (0.26G)	30.02 (0.53G)	21.59 (1.23G)	17.52 (4.15G)
APOLLO-1/8	32.50 (0.26G)	23.74 (0.53G)	16.98 (1.23G)	14.32 (4.15G)
GWT-3	29.81 (0.26G)	22.63 (0.51G)	16.35 (1.09G)	13.48 (3.80G)
Fira* [9]	31.06 (0.26G)	22.73 (0.52G)	17.03 (1.23G)	14.31 (4.15G)
LoRA* [7]	34.99 (0.37G)	33.92 (0.81G)	25.58 (1.76G)	19.21 (6.17G)
ReLoRA* [7]	37.04 (0.37G)	29.37 (0.81G)	29.08 (1.76G)	18.33 (6.17G)
Training Tokens	1.3B	2.6B	7.8B	13.1B

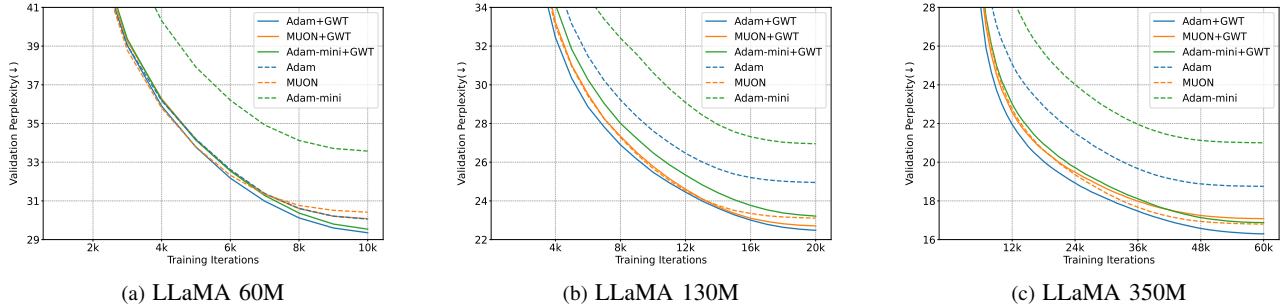


Fig. 4. Applying GWT to Adam/Adam-mini/MUON optimizers for pre-training various LLaMA models. GWT is scalable to optimizers beyond Adam and consistently achieves lower or comparable PPL than full-rank methods across all tested optimizers.

configurations that use 2-level and 3-level decompositions. Following prior work [7], [9], [14], we adopt the same module-wise optimizer initialization strategy that applies GWT to both the Multi-Layer Perceptron (MLP) and attention modules of the transformer, while the remaining modules are optimized with Adam.

GWT is effective in pre-training. The final validation perplexity (PPL) and estimated memory usage for all methods are summarized in Table II. Experimental results show that GWT consistently achieves lower validation PPL while reducing memory usage (model + optimizer states, BF16) compared to other memory-efficient baselines. In all the pre-training cases, GWT outperforms full-rank optimizers. Specifically, in the LLaMA 1B pre-training experiment, our 3-level GWT method reduces the total memory cost by 52% and the optimizer memory cost by 79% (from 7.80GB to 3.81GB on LLaMA 1B). Even with the use of 2-level GWT, our method still achieves experimental results that surpass full-rank, while reducing total memory consumption by up to 45%. In the same scenario, the gap between GaLore-1/8 and full-rank is further widened. Details of the memory estimation are presented in the Appendix.

GWT leads to faster convergence. We present learning

curves for the pre-training task on LLaMA 60M-350M in Figure 4. These curves show that GWT consistently outperforms both full-rank Adam and GaLore across different levels of wavelet transformation. In most cases, GaLore consistently shows a significant gap compared to full-rank Adam, while all GWT methods maintain results surpassing full-rank. Moreover, GWT not only achieves lower final validation PPL but also accelerates convergence compared to the baselines.

GWT is optimizer-agnostic. We extend our method to the Adam-mini [28] and MUON [19] optimizers and present the corresponding experimental results in Figure 4. Similar to its performance with Adam, GWT continues to achieve results comparable to or better than the full-rank methods. This highlights the versatility and effectiveness of our method when integrated with other optimizers, showcasing its broad applicability in memory-efficient optimization.

GWT achieves higher training throughput. In addition to evaluating final validation perplexity and memory consumption, we also measure token throughput during the pre-training of the LLaMA-3B model using GWT-2, GaLore-1/4, APOLLO-1/4, and 8-bit Adam. The results are presented in Table III. Our method, GWT-2, achieves a training throughput of 0.532K tokens per second per GPU, delivering over a 1.9×

TABLE III
PRE-TRAINING LLAMA 3B ON C4. WE REPORT THE VALIDATION PPL ON DIFFERENT ITERATIONS AND THE TOKEN THROUGHPUT PER GPU.

	20K	40K	60K	80K	100K	120K	Tokens/s	Time	Mem.
Full-Rank Adam	Out of Memory						-	-	16.0G
8bit-Adam	21.79	17.44	15.70	14.99	14.52	14.31	0.274K	541.9h	10.7G
GaLore-1/4	20.42	17.36	15.98	15.12	14.79	14.73	0.526K	335.4h	9.28G
APOLLO-1/4	20.78	17.19	15.40	14.40	13.90	13.75	0.541K	274.4h	9.28G
GWT-2	19.74	16.41	14.80	13.77	13.46	13.21	0.532K	279.1h	8.54G
Tokens (B)	2.6	5.2	7.8	10.4	13.1	15.7			

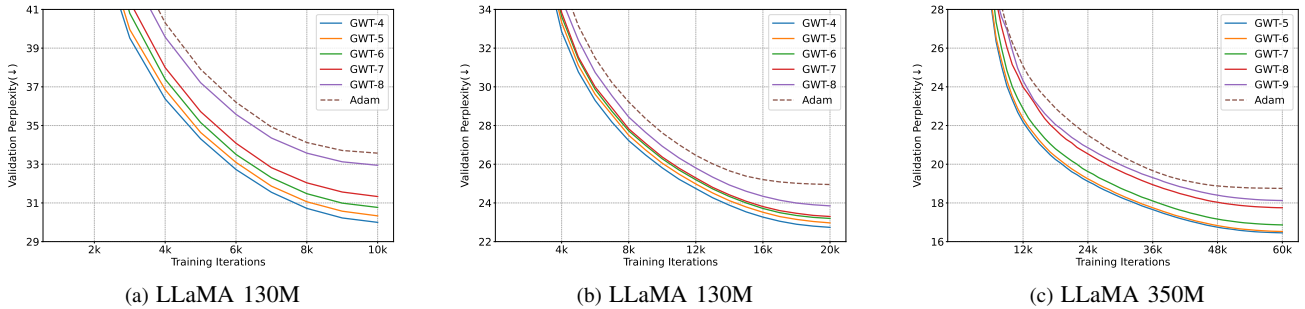


Fig. 5. **Applying GWT to Adam for pre-training LLaMA models with reduced memory usage (higher l).** GWT maintains superior performance over Adam under high wavelet transform l levels.

speedup compared to 8-bit Adam [24], and approximately a 6% improvement over GaLore. Furthermore, GWT-2 achieves throughput comparable to the SVD-free APOLLO method, highlighting its efficiency in large-scale model training.

GWT is robust to long sequence lengths. We evaluate GWT in handling longer sequences (512, 1024) while keeping the total number of training tokens per batch constant. Table IV reports the final validation PPL across different methods. In contrast to GaLore, which exhibits noticeable performance degradation as sequence length increases, GWT maintains stable performance, showing only a slight increase in PPL. This resilience highlights GWT as a promising candidate for partial LLM pre-training scenarios, i.e., long-context windows and trillions of training tokens.

TABLE IV
FINAL VALIDATION PPL ON PRE-TRAINING LLAMA MODELS WITH DIFFERENT SEQUENCE LENGTH.

Models	60M		130M		350M	
	512	1024	512	1024	512	1024
Full-Rank Adam	34.55	37.52	25.95	28.12	19.95	22.02
GaLore-1/4	40.25	42.02	27.19	33.97	19.92	21.73
APOLLO-1/4	32.29	34.64	24.02	25.93	17.26	18.77
GWT-2	30.12	32.55	23.01	24.89	16.68	18.21

GWT remains efficient under SGD-level memory constraints. We assess the performance of GWT at higher decomposition levels, as illustrated in Figure 5. Notably, even at extreme levels (e.g., $l = 7, 8, 9$), where the memory footprint of the optimizer approaches that of SGD, GWT consistently outperforms full-rank Adam in terms of validation

TABLE V
COMPARISON RESULTS OF VARIOUS FINE-TUNING ALGORITHMS ON MMLU TASKS.

Models	Methods	STEM	Social Sciences	Humanities	Other	Avg.
LLaMA3.2-3B	Adam	49.50	68.25	56.28	64.74	59.40
	LoRA	49.83	67.63	56.56	63.88	59.23
	GaLore	49.73	68.70	55.94	64.47	59.37
	APOLLO	49.17	68.18	56.32	64.71	59.32
	GWT	49.50	68.61	56.56	64.62	59.34
Gemma3-4B	Adam	46.59	64.74	49.71	58.91	54.46
	LoRA	45.36	63.41	48.63	58.36	53.41
	GaLore	46.36	64.51	49.42	58.91	54.26
	APOLLO	46.49	64.28	49.39	58.67	54.17
	GWT	46.39	64.87	49.73	59.38	54.56
Qwen2.5-7B	Adam	-	-	-	-	OOM
	LoRA	70.44	83.23	67.80	76.90	73.85
	GaLore	70.21	83.49	67.52	76.87	73.76
	APOLLO	70.51	83.43	67.35	76.96	73.77
	GWT	70.38	83.88	68.06	77.14	74.12

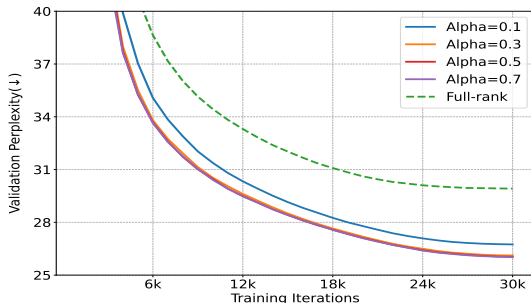
PPL, demonstrating its robustness and effectiveness in low-memory training regimes.

B. Memory-Efficient Fine-Tuning

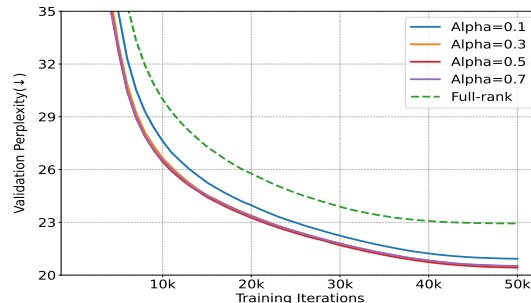
In this section, we further evaluate the effectiveness of our method by fine-tuning the LLaMA-3.2-3B [33], Gemma3-4B [34], and Qwen2.5-7B [35] models, and report their performance on the MMLU benchmark [31]. For a fair comparison, LoRA, GaLore, and APOLLO are configured with a rank of 8, while GWT is set to a decomposition level of 8 to ensure memory alignment across methods. We report the best accuracy achieved by sweeping the learning rate among $[1.0e-6, 2.5e-6, 5.0e-6, 1.0e-5, 2.5e-5, 5.0e-5, 1.0e-4]$, which ensures a fair evaluation for optimizers with different sensitivities to learning rates. Additionally, to provide a more comprehensive

TABLE VI
FINE-TUNING ON GLUE BENCHMARK USING PRE-TRAINED ROBERTA-BASE MODEL.

	CoLA	STS-B	MRPC	RTE	SST2	MNLI	QNLI	QQP	Avg.
Adam	63.81	91.26	92.25	79.06	94.57	87.29	92.18	92.28	86.58
GaLore	61.32	91.13	92.41	77.25	94.03	86.77	92.56	91.77	85.90
APOLLO	61.07	90.70	92.00	78.33	93.57	87.21	92.27	91.85	85.87
LoRA* [7]	61.83	90.80	91.90	79.06	93.46	86.94	92.25	91.22	85.93
GWT	62.57	91.16	93.26	79.42	94.26	87.37	92.53	91.94	86.56



(a) LLaMA 60M



(b) LLaMA 130M

Fig. 6. Study the effects of α on pre-training LLaMA 60M and 130M models.

assessment, we include results from fine-tuning the RoBERTa-base model [36] on the GLUE [32], [37]–[42] in Table VI.

GWT is effective in fine-tuning. We report the MMLU results in Table V and the GLUE results in Table VI. As shown, GWT consistently matches or exceeds the performance of the baselines. These results demonstrate that GWT is not only effective during pre-training but also excels in fine-tuning scenarios, achieving competitive performance across diverse tasks while maintaining memory efficiency.

C. Study the Effect of α

Similar to other memory-efficient optimizers [7], [9], [14], GWT introduces an additional hyperparameter α to control the effective learning rate of the GWT module. In this section, we investigate the impact of this hyperparameter on the performance of GWT. We evaluate Adam with a 2-level Haar GWT across different values of α while fixing the learning rate at $lr = 0.01$. As shown in Figure 6, our results indicate that GWT performance is largely invariant to the choice of α . In particular, for $\alpha > 0.1$, the final performance remains stable with no significant differences. Under our module-wise optimizer strategy, most network modules operate with an effective learning rate greater than $0.001 (lr \times \alpha)$. In contrast, Adam typically requires learning rates smaller than 0.001 to prevent loss spikes. This highlights the superior robustness of GWT to higher learning rates. Furthermore, in fine-tuning tasks, tuning α effectively corresponds to adjusting the learning rate lr under our strategy. A more detailed study of the interaction between lr and α in fine-tuning settings is provided in the Appendix.

D. Extend to GPT and Qwen Models

In this section, we extend GWT to models beyond pre-training LLaMA, where we pre-train GPT-2 [3], DeBERTa [43], and Qwen2.5-0.5B [35] on the C4 dataset with 2.6B tokens. The final validation loss results are presented in Table VII. We can see that GWT still maintains superior performance in terms of PPL across the tested models, demonstrating its effectiveness on other LLM architectures and its strength as a choice for LLM pre-training.

TABLE VII
FINAL VALIDATION LOSS ON GPT, DEBERTA, AND QWEN.

Methods	GPT	DeBERTa	Qwen
Full-rank Adam	3.31	2.16	2.85
GaLore-1/4	3.43	2.22	2.97
APOLLO	3.26	2.07	2.82
GWT-2	3.22	2.02	2.70

V. DISCUSSIONS

Our proposed GWT and its implementation draw inspiration from GaLore [7]. Both GWT and GaLore are closely related to Projected Gradient Descent (PGD) [44], [45], which projects the gradient onto a subspace before performing the update. However, there are key distinctions between GWT and GaLore. The primary difference lies in the projection operation: GWT not only projects the gradient onto the subspace but also leverages additional information from this projection, such as the detail coefficients D_t (as shown in Eq. (6)). In contrast, GaLore discards the remaining information after projecting the gradient onto the subspace. When projecting back from

the subspace to the gradient space, GWT retains more of the original gradient information. Importantly, this additional information is temporary and generated during the wavelet transform process itself, so it does not require extra storage. In summary, GWT provides an effective solution to the memory challenges encountered in training large models.

Here, we outline several intriguing open problems related to GWT: (a) Wavelets are originally designed for time-series signals and images, raising the question: Can a specialized wavelet transform be developed to handle gradients, which are inherently more disordered and chaotic? Additionally, since the impact of l on the experimental results is minimal, the main effect of higher-order GWT lies in throughput, while offering higher memory efficiency. Therefore, the potential of GWT with higher l values is worth exploring. Given the linear properties of the Haar wavelet in GWT, is it possible to accelerate multi-level wavelet transforms to achieve even higher memory compression ratios, such as 1/64 or 1/128? (b) The applicability and effectiveness of GWT in other domains, such as vision models [46] and diffusion models [47], [48], remain to be validated.

VI. CONCLUSION

In this paper, we explore memory-efficient optimization algorithms that go beyond traditional low-rank decomposition and system-level techniques. Drawing inspiration from the limitations of current optimization methods, we propose a novel optimizer state memory compression method that integrates WT into gradients. This method bridges the gap between gradient compression and wavelet transforms, enabling more efficient training of LLMs by reducing memory usage and accelerating training speed. Our experimental results demonstrate that GWT achieves performance comparable to that of advanced memory-efficient optimizers and full-rank methods across various LLM training stages. This gradient compression technique not only improves final validation scores but also accelerates training convergence and increases throughput. Moreover, this method is applicable to existing memory-intensive optimizers beyond Adam. In summary, our approach validates the feasibility of applying wavelet transforms to enhance the training efficiency of LLMs, providing a novel perspective on designing memory-efficient algorithms that effectively address the memory bottleneck in LLM training.

REFERENCES

- [1] T. B. Brown, B. Mann, N. Ryder, M. Subbiah, J. Kaplan, P. Dhariwal, A. Neelakantan, P. Shyam, G. Sastry, A. Askell, S. Agarwal, A. Herbert-Voss, G. Krueger, T. Henighan, R. Child, A. Ramesh, D. M. Ziegler, J. Wu, C. Winter, C. Hesse, M. Chen, E. Sigler, M. Teusz Litwin, S. Gray, B. Chess, J. Clark, C. Berner, S. McCandlish, A. Radford, I. Sutskever, and D. Amodei, "Language models are few-shot learners," *ArXiv*, vol. abs/2005.14165, 2020.
- [2] A. Vaswani, N. Shazeer, N. Parmar, J. Uszkoreit, L. Jones, A. N. Gomez, E. Kaiser, and I. Polosukhin, "Attention is all you need," *Advances in neural information processing systems*, vol. 30, 2017.
- [3] A. Radford, J. Wu, R. Child, D. Luan, D. Amodei, I. Sutskever *et al.*, "Language models are unsupervised multitask learners," *OpenAI blog*, vol. 1, no. 8, p. 9, 2019.
- [4] H. Touvron, L. Martin, K. R. Stone, P. Albert, and e. a. Amjad Almahairi, "Llama 2: Open foundation and fine-tuned chat models," *ArXiv*, vol. abs/2307.09288, 2023.
- [5] A. Liu, B. Feng, B. Xue, B. Wang, B. Wu, C. Lu, C. Zhao, C. Deng, C. Zhang, C. Ruan *et al.*, "Deepseek-v3 technical report," *arXiv preprint arXiv:2412.19437*, 2024.
- [6] D. P. Kingma and J. Ba, "Adam: A method for stochastic optimization," *CoRR*, vol. abs/1412.6980, 2014.
- [7] J. Zhao, Z. Zhang, B. Chen, Z. Wang, A. Anandkumar, and Y. Tian, "Galore: Memory-efficient llm training by gradient low-rank projection," *arXiv preprint arXiv:2403.03507*, 2024.
- [8] E. J. Hu, Y. Shen, P. Wallis, Z. Allen-Zhu, Y. Li, S. Wang, L. Wang, W. Chen *et al.*, "Lora: Low-rank adaptation of large language models," *ICLR*, vol. 1, no. 2, p. 3, 2022.
- [9] X. Chen, K. Feng, C. Li, X. Lai, X. Yue, Y. Yuan, and G. Wang, "Fira: Can we achieve full-rank training of llms under low-rank constraint?" *ArXiv*, vol. abs/2410.01623, 2024.
- [10] W. Xia, C. Qin, and E. Hazan, "Chain of lora: Efficient fine-tuning of language models via residual learning," *arXiv preprint arXiv:2401.04151*, 2024.
- [11] L. Zhang, L. Zhang, S. Shi, X. Chu, and B. Li, "Lora-fa: Memory-efficient low-rank adaptation for large language models fine-tuning," *arXiv preprint arXiv:2308.03303*, 2023.
- [12] Y. Hao, Y. Cao, and L. Mou, "Flora: Low-rank adapters are secretly gradient compressors," *arXiv preprint arXiv:2402.03293*, 2024.
- [13] Y. He, P. Li, Y. Hu, C. Chen, and K. Yuan, "Subspace optimization for large language models with convergence guarantees," *arXiv preprint arXiv:2410.11289*, 2024.
- [14] H. Zhu, Z. Zhang, W. Cong, X. Liu, S. Park, V. Chandra, B. Long, D. Z. Pan, Z. Wang, and J. Lee, "Apollo: Sgd-like memory, adamw-level performance," 2024.
- [15] O. Rioul and M. Vetterli, "Wavelets and signal processing," *IEEE Signal Processing Magazine*, vol. 8, no. 4, pp. 14–38, 1991.
- [16] V. Lialin, N. Shivagunde, S. Muckatira, and A. Rumshisky, "Relora: High-rank training through low-rank updates, 2023," *URL https://arxiv.org/abs/2307.05695*, 2023.
- [17] S.-Y. Liu, C.-Y. Wang, H. Yin, P. Molchanov, Y.-C. F. Wang, K.-T. Cheng, and M.-H. Chen, "Dora: Weight-decomposed low-rank adaptation," in *Forty-first International Conference on Machine Learning*, 2024.
- [18] T. Robert, M. Safaryan, I.-V. Modoranu, and D. Alistarh, "LDAdam: Adaptive optimization from low-dimensional gradient statistics," in *The Thirteenth International Conference on Learning Representations*, 2025.
- [19] J. Liu, J. Su, X. Yao, Z. Jiang, G. Lai, Y. Du, Y. Qin, W. Xu, E. Lu, J. Yan *et al.*, "Muon is scalable for llm training," *arXiv preprint arXiv:2502.16982*, 2025.
- [20] C. Ma, W. Gong, M. Scetbon, and E. Meeds, "Swan: Sgd with normalization and whitening enables stateless llm training," *ArXiv*, vol. abs/2412.13148, 2024.
- [21] M. Scetbon, C. Ma, W. Gong, and E. Meeds, "Gradient multi-normalization for stateless and scalable llm training," *arXiv preprint arXiv:2502.06742*, 2025.
- [22] A. Glentis, J. Li, A. Han, and M. Hong, "A minimalist optimizer design for LLM pretraining," in *ES-FoMo III: 3rd Workshop on Efficient Systems for Foundation Models*, 2025.
- [23] T. Chen, B. Xu, C. Zhang, and C. Guestrin, "Training deep nets with sublinear memory cost," *arXiv preprint arXiv:1604.06174*, 2016.
- [24] T. Dettmers, M. Lewis, S. Shleifer, and L. Zettlemoyer, "8-bit optimizers via block-wise quantization," *arXiv preprint arXiv:2110.02861*, 2021.
- [25] T. Dettmers, A. Pagnoni, A. Holtzman, and L. Zettlemoyer, "Qlora: Efficient finetuning of quantized llms," *Advances in Neural Information Processing Systems*, vol. 36, 2024.
- [26] P. Porwik and A. Lisowska, "The haar-wavelet transform in digital image processing: Its status and achievements," *Machine graphics & vision*, vol. 13, pp. 79–98, 2004.
- [27] I. Molybog, P. Albert, M. Chen, Z. DeVito, D. Esiobu, N. Goyal, P. S. Koura, S. Narang, A. Poulton, R. Silva, B. Tang, D. Liskovich, P. Xu, Y. Zhang, M. H. M. Kambadur, S. Roller, and S. Zhang, "A theory on adam instability in large-scale machine learning," *ArXiv*, vol. abs/2304.09871, 2023.
- [28] Y. Zhang, C. Chen, Z. Li, T. Ding, C. Wu, D. P. Kingma, Y. Ye, Z.-Q. Luo, and R. Sun, "Adam-mini: Use fewer learning rates to gain more," *arXiv preprint arXiv:2406.16793*, 2024.
- [29] H. Touvron, T. Lavril, G. Izacard, X. Martinet, M.-A. Lachaux, T. Lacroix, B. Rozière, N. Goyal, E. Hambro, F. Azhar, A. Rodriguez, A. Joulin, E. Grave, and G. Lample, "Llama: Open and efficient foundation language models," *ArXiv*, vol. abs/2302.13971, 2023.
- [30] C. Raffel, N. M. Shazeer, A. Roberts, K. Lee, S. Narang, M. Matena, Y. Zhou, W. Li, and P. J. Liu, "Exploring the limits of transfer learning

- with a unified text-to-text transformer,” *J. Mach. Learn. Res.*, vol. 21, pp. 140:1–140:67, 2019.
- [31] D. Hendrycks, C. Burns, S. Basart, A. Zou, M. Mazeika, D. Song, and J. Steinhardt, “Measuring massive multitask language understanding,” *arXiv preprint arXiv:2009.03300*, 2020.
- [32] A. Wang, A. Singh, J. Michael, F. Hill, O. Levy, and S. R. Bowman, “Glue: A multi-task benchmark and analysis platform for natural language understanding,” *arXiv preprint arXiv:1804.07461*, 2018.
- [33] A. Grattafiori, A. Dubey, A. Jauhri, A. Pandey, A. Kadian, A. Al-Dahle, A. Letman, A. Mathur, A. Schelten, A. Vaughan *et al.*, “The llama 3 herd of models,” *arXiv preprint arXiv:2407.21783*, 2024.
- [34] G. Team, A. Kamath, J. Ferret, S. Pathak, N. Vieillard, R. Merhej, S. Perrin, T. Matejovicova, A. Ramé, M. Rivière *et al.*, “Gemma 3 technical report,” *arXiv preprint arXiv:2503.19786*, 2025.
- [35] A. Yang, B. Yang, B. Zhang, B. Hui, B. Zheng, B. Yu, C. Li, D. Liu, F. Huang, H. Wei *et al.*, “Qwen2. 5 technical report,” *arXiv preprint arXiv:2412.15115*, 2024.
- [36] Y. Liu, “Roberta: A robustly optimized bert pretraining approach,” *arXiv preprint arXiv:1907.11692*, vol. 364, 2019.
- [37] A. Warstadt, A. Singh, and S. R. Bowman, “Neural network acceptability judgments,” *Transactions of the Association for Computational Linguistics*, vol. 7, pp. 625–641, 2018.
- [38] D. M. Cer, M. T. Diab, E. Agirre, I. Lopez-Gazpio, and L. Specia, “Semeval-2017 task 1: Semantic textual similarity multilingual and crosslingual focused evaluation,” in *International Workshop on Semantic Evaluation*, 2017.
- [39] W. B. Dolan and C. Brockett, “Automatically constructing a corpus of sentential paraphrases,” in *International Joint Conference on Natural Language Processing*, 2005.
- [40] R. Socher, A. Perelygin, J. Wu, J. Chuang, C. D. Manning, A. Ng, and C. Potts, “Recursive deep models for semantic compositionality over a sentiment treebank,” in *Conference on Empirical Methods in Natural Language Processing*, 2013.
- [41] A. Williams, N. Nangia, and S. R. Bowman, “A broad-coverage challenge corpus for sentence understanding through inference,” in *North American Chapter of the Association for Computational Linguistics*, 2017.
- [42] P. Rajpurkar, R. Jia, and P. Liang, “Know what you don’t know: Unanswerable questions for squad,” *ArXiv*, vol. abs/1806.03822, 2018.
- [43] P. He, X. Liu, J. Gao, and W. Chen, “Deberta: Decoding-enhanced bert with disentangled attention,” 2021.
- [44] H. Chen, G. Raskutti, and M. Yuan, “Non-convex projected gradient descent for generalized low-rank tensor regression,” *J. Mach. Learn. Res.*, vol. 20, pp. 5:1–5:37, 2016.
- [45] Y. Chen and M. J. Wainwright, “Fast low-rank estimation by projected gradient descent: General statistical and algorithmic guarantees,” *ArXiv*, vol. abs/1509.03025, 2015.
- [46] A. Dosovitskiy, L. Beyer, A. Kolesnikov, D. Weissenborn, X. Zhai, T. Unterthiner, M. Dehghani, M. Minderer, G. Heigold, S. Gelly, J. Uszkoreit, and N. Houlsby, “An image is worth 16x16 words: Transformers for image recognition at scale,” *ICLR*, 2021.
- [47] J. Ho, A. Jain, and P. Abbeel, “Denoising diffusion probabilistic models,” *Advances in neural information processing systems*, vol. 33, pp. 6840–6851, 2020.
- [48] Y. Song, J. Sohl-Dickstein, D. P. Kingma, A. Kumar, S. Ermon, and B. Poole, “Score-based generative modeling through stochastic differential equations,” *arXiv preprint arXiv:2011.13456*, 2020.
- [49] A. Jacot, F. Gabriel, and C. Hongler, “Neural tangent kernel: Convergence and generalization in neural networks,” *Advances in neural information processing systems*, vol. 31, 2018.
- [50] S. Arora, S. Du, W. Hu, Z. Li, and R. Wang, “Fine-grained analysis of optimization and generalization for overparameterized two-layer neural networks,” in *International conference on machine learning*. PMLR, 2019, pp. 322–332.
- [51] Z. Allen-Zhu, Y. Li, and Z. Song, “A convergence theory for deep learning via over-parameterization,” in *Proceedings of the 36th International Conference on Machine Learning*, ser. Proceedings of Machine Learning Research, vol. 97. PMLR, Jun. 2019, pp. 242–252. [Online]. Available: <https://proceedings.mlr.press/v97/allen-zhu19a.html>
- [52] K. He, X. Zhang, S. Ren, and J. Sun, “Delving deep into rectifiers: Surpassing human-level performance on imagenet classification,” in *Proceedings of the IEEE international conference on computer vision*, 2015, pp. 1026–1034.
- [53] A. Bietti and J. Mairal, “On the inductive bias of neural tangent kernels,” *Advances in Neural Information Processing Systems*, vol. 32, 2019.
- [54] Y. Zheng, R. Zhang, J. Zhang, Y. Ye, Z. Luo, Z. Feng, and Y. Ma, “Llamafactory: Unified efficient fine-tuning of 100+ language models,” *arXiv preprint arXiv:2403.13372*, 2024.
- [55] R. Taori, I. Gulrajani, T. Zhang, Y. Dubois, X. Li, C. Guestrin, P. Liang, and T. B. Hashimoto, “Stanford alpaca: An instruction-following llama model,” https://github.com/tatsu-lab/stanford_alpaca, 2023.
- [56] A. Paszke, S. Gross, S. Chintala, G. Chanan, E. Yang, Z. DeVito, Z. Lin, A. Desmaison, L. Antiga, and A. Lerer, “Automatic differentiation in pytorch,” 2017.
- [57] M. Wolter, F. Blanke, J. Garcke, and C. T. Hoyt, “ptwt - the pytorch wavelet toolbox,” *Journal of Machine Learning Research*, vol. 25, no. 80, pp. 1–7, 2024.
- [58] K. Everett, L. Xiao, M. Wortsman, A. Alemi, R. Novak, P. J. Liu, I. Gur, J. N. Sohl-Dickstein, L. P. Kaelbling, J. Lee, and J. Pennington, “Scaling exponents across parameterizations and optimizers,” *ArXiv*, vol. abs/2407.05872, 2024.
- [59] R. Genet and H. Inzirillo, “Caadam: Improving adam optimizer using connection aware methods,” *ArXiv*, vol. abs/2410.24216, 2024.

APPENDIX A
WHY HAAR WAVELET IS BETTER

Lemma 1. Let $x = (x_1, \dots, x_b) \in \mathbb{R}^b$ and let $\bar{x} := \frac{1}{b} \sum_{j=1}^b x_j$. Define the difference operator $D : \mathbb{R}^b \rightarrow \mathbb{R}^{b-1}$ by

$$(Dx)_j := x_{j+1} - x_j, \quad j = 1, \dots, b-1.$$

Then

$$\|x - \bar{x} \mathbf{1}\|_2 \leq \kappa_b \|Dx\|_2,$$

with

$$\kappa_b := \frac{1}{\sqrt{2(1 - \cos(\pi/b))}} = \frac{1}{2 \sin(\pi/(2b))}.$$

Proof. Let $L := D^\top D \in \mathbb{R}^{b \times b}$, i.e., L is the path-graph Laplacian:

$$L = \begin{pmatrix} 1 & -1 & 0 & \cdots & 0 \\ -1 & 2 & -1 & \ddots & \vdots \\ 0 & -1 & 2 & \ddots & 0 \\ \vdots & \ddots & \ddots & \ddots & -1 \\ 0 & \cdots & 0 & -1 & 1 \end{pmatrix},$$

$$x^\top Lx = \|Dx\|_2^2 = \sum_{j=1}^{b-1} (x_{j+1} - x_j)^2$$

Define, for $k = 0, 1, \dots, b-1$, vectors $v^{(k)} \in \mathbb{R}^b$ by

$$v_j^{(k)} := \cos\left(\left(j - \frac{1}{2}\right) \frac{k\pi}{b}\right), \quad j = 1, \dots, b.$$

Let $\alpha := \frac{k\pi}{b}$. Using the identity

$$\cos\left(\left(j + \frac{1}{2}\right)\alpha\right) + \cos\left(\left(j - \frac{3}{2}\right)\alpha\right) = 2 \cos(\alpha) \cos\left(\left(j - \frac{1}{2}\right)\alpha\right),$$

one checks for interior indices $2 \leq j \leq b-1$ that

$$(Lv^{(k)})_j = 2v_j^{(k)} - v_{j-1}^{(k)} - v_{j+1}^{(k)} = 2(1 - \cos(\alpha))v_j^{(k)}.$$

For the endpoints, using $\cos u - \cos v = 2 \sin\left(\frac{u+v}{2}\right) \sin\left(\frac{v-u}{2}\right)$, we get

$$\begin{aligned} (Lv^{(k)})_1 &= v_1^{(k)} - v_2^{(k)} = \cos\left(\frac{\alpha}{2}\right) - \cos\left(\frac{3\alpha}{2}\right) \\ &= 2(1 - \cos(\alpha)) \cos\left(\frac{\alpha}{2}\right) = 2(1 - \cos(\alpha))v_1^{(k)}, \end{aligned}$$

and similarly $(Lv^{(k)})_b = 2(1 - \cos(\alpha))v_b^{(k)}$. Hence $v^{(k)}$ is an eigenvector of L with eigenvalue

$$\lambda_k = 2(1 - \cos(k\pi/b)), \quad k = 0, 1, \dots, b-1.$$

In particular, $\lambda_0 = 0$ with eigenvector $v^{(0)} = \mathbf{1}$, and the smallest positive eigenvalue is

$$\lambda_1 = 2(1 - \cos(\pi/b)).$$

Now let $y := x - \bar{x} \mathbf{1}$. Then $y \perp \mathbf{1}$ and $Dy = Dx$. Expand y in the orthogonal eigenbasis $\{v^{(k)}\}_{k=0}^{b-1}$: $y = \sum_{k=1}^{b-1} c_k v^{(k)}$ (no $k=0$ term since $y \perp \mathbf{1}$). Then

$$y^\top Ly = \sum_{k=1}^{b-1} \lambda_k c_k^2 \geq \lambda_1 \sum_{k=1}^{b-1} c_k^2 = \lambda_1 \|y\|_2^2.$$

Therefore,

$$\|x - \bar{x} \mathbf{1}\|_2^2 = \|y\|_2^2 \leq \frac{1}{\lambda_1} y^\top Ly = \frac{1}{\lambda_1} \|Dy\|_2^2 = \frac{1}{\lambda_1} \|Dx\|_2^2,$$

which proves the claim with $\kappa_b = 1/\sqrt{\lambda_1}$. □

Lemma 2. With the notation of Theorem 1, one has

$$\|G - P_l(G)\|_F \leq \kappa_b \|\Delta G\|_F.$$

Proof. Fix a row index $i \in \{1, \dots, m\}$ and a block \mathcal{B}_k . Let $x \in \mathbb{R}^b$ be the length- b vector formed by the entries of the i -th row restricted to \mathcal{B}_k : $x_t := G_{i,(k-1)b+t}$ for $t = 1, \dots, b$. Then $(P_l(G))_{i,(k-1)b+t} = \bar{x}$ for all t , where \bar{x} is the mean of x . Applying Lemma 1 to this x yields

$$\begin{aligned} & \sum_{t=1}^b (G_{i,(k-1)b+t} - (P_l(G))_{i,(k-1)b+t})^2 \\ & \leq \kappa_b^2 \sum_{t=1}^{b-1} (G_{i,(k-1)b+t+1} - G_{i,(k-1)b+t})^2. \end{aligned}$$

Summing over all blocks $k = 1, \dots, q$ and all rows $i = 1, \dots, m$ gives

$$\|G - P_l(G)\|_F^2 \leq \kappa_b^2 \sum_{i=1}^m \sum_{k=1}^q \sum_{t=1}^{b-1} (G_{i,(k-1)b+t+1} - G_{i,(k-1)b+t})^2.$$

The triple sum on the right only includes within-block adjacent differences, hence it is at most $\sum_{i=1}^m \sum_{j=1}^{n-1} (G_{i,j+1} - G_{i,j})^2 = \|\Delta G\|_F^2$. Taking square roots yields the result. \square

Lemma 3 (Main Lemma). *Let $G \in \mathbb{R}^{m \times n}$ and fix an integer level $l \geq 0$ with block length $b := 2^l$ dividing n . Partition the column indices into $q := n/b$ consecutive blocks $\mathcal{B}_k := \{(k-1)b + 1, \dots, kb\}$. Define the block-averaging (Haar low-pass) operator $P_l : \mathbb{R}^{m \times n} \rightarrow \mathbb{R}^{m \times n}$ by*

$$(P_l(G))_{:,j} := \bar{g}_k \text{ for } j \in \mathcal{B}_k, \quad \bar{g}_k := \frac{1}{b} \sum_{t \in \mathcal{B}_k} G_{:,t} \in \mathbb{R}^m.$$

Denote the column difference operator $\Delta : \mathbb{R}^{m \times n} \rightarrow \mathbb{R}^{m \times (n-1)}$ be

$$(\Delta G)_{:,j} := G_{:,j+1} - G_{:,j}, \quad j = 1, \dots, n-1.$$

Assume that for some integer $r \geq 0$,

$$\|\Delta G\|_F < \left[\sin\left(\frac{\pi}{b}\right) \sqrt{r} \right] \sigma_{r+1}(G), \quad (\text{Assumption PS})$$

where $\sigma_{r+1}(G)$ is the $(r+1)$ -th singular value of G . Then the Haar level- l low-pass approximation $P_l(G)$ (that is, Haar wavelet detail coefficients set to zero at scales $\leq l$) satisfies the strict comparison

$$\|G - P_l(G)\|_F < \inf_{\text{rank}(X) \leq r} \|G - X\|_F.$$

Proof. Note that Eq. (Assumption PS) yields

$$\kappa_b \|\Delta G\|_F < \sqrt{r} \sigma_{r+1}(G).$$

By Lemma 2,

$$\|G - P_l(G)\|_F \leq \kappa_b \|\Delta G\|_F.$$

With direct computations,

$$\inf_{\text{rank}(X) \leq r} \|G - X\|_F = \left(\sum_{k>r} \sigma_k(G)^2 \right)^{1/2} \geq \sqrt{r} \sigma_{r+1}(G).$$

Under (Assumption PS), we thus have

$$\begin{aligned} \|G - P_l(G)\|_F & \leq \kappa_b \|\Delta G\|_F < \sqrt{r} \sigma_{r+1}(G) \\ & \leq \inf_{\text{rank}(X) \leq r} \|G - X\|_F, \end{aligned}$$

which is the claimed strict dominance. \square

Discussions. In LLM training, a commonly used setting is $m = n$, $r = \frac{n}{4}$ and $l = 3$, the Eq. (Assumption PS) reduces to

$$\|\Delta G\|_F < [0.1913\sqrt{n}] \sigma_{r+1}(G),$$

where the column difference operator $\Delta : \mathbb{R}^{m \times n} \rightarrow \mathbb{R}^{m \times (n-1)}$ be

$$(\Delta G)_{:,j} := G_{:,j+1} - G_{:,j}, \quad j = 1, \dots, n-1.$$

APPENDIX B
THEORETICAL ANALYSIS OF GRADIENT LOW-RANK STRUCTURE

In this section, we establish rigorous theoretical foundations showing that the gradient matrix arising from training over-parameterized Transformers satisfies the low-rank condition required by our algorithm. Throughout this section, we use $\|\cdot\|_F$ and $\|\cdot\|_2$ to denote the Frobenius norm and spectral norm, respectively. For a matrix M , we denote its k -th largest singular value by $\sigma_k(M)$.

A. Model and Notation

We consider a simplified single-head self-attention layer followed by a linear projection:

$$f(X; \theta) = \underbrace{\text{softmax}\left(\frac{XW_QW_K^\top X^\top}{\sqrt{d_k}}\right)}_{=: A(X; \theta) \in \mathbb{R}^{n \times n}} XW_VW_O, \quad (7)$$

where:

- $X \in \mathbb{R}^{n \times d}$ is the input sequence matrix with n tokens each of dimension d ;
- $W_Q, W_K \in \mathbb{R}^{d \times d_k}$ are the query and key projection matrices;
- $W_V \in \mathbb{R}^{d \times d_v}$ is the value projection matrix;
- $W_O \in \mathbb{R}^{d_v \times d_o}$ is the output projection matrix;
- $\theta = (W_Q, W_K, W_V, W_O)$ denotes the collection of all trainable parameters;
- $m = 2d \cdot d_k + d \cdot d_v + d_v \cdot d_o$ is the total number of parameters;
- $d_{\min} := \min\{d_k, d_v\}$ is defined as the model width.

Given a training set $\{(X^{(i)}, y^{(i)})\}_{i=1}^N$ and a differentiable loss function $\ell : \mathbb{R}^{d_o} \times \mathbb{R}^{d_o} \rightarrow \mathbb{R}_{\geq 0}$, we define the per-sample loss as $L_i(\theta) = \ell(f(X^{(i)}; \theta), y^{(i)})$.

Definition 2 (Gradient Matrix). The gradient matrix $G \in \mathbb{R}^{m \times n}$ is defined as

$$G := [\text{vec}(\nabla_{\theta} L_1) \quad \text{vec}(\nabla_{\theta} L_2) \quad \cdots \quad \text{vec}(\nabla_{\theta} L_N)], \quad (8)$$

where $\text{vec}(\cdot)$ denotes the vectorization operator.

Definition 3 (Column Difference Operator). The column difference operator $\Delta : \mathbb{R}^{m \times N} \rightarrow \mathbb{R}^{m \times (N-1)}$ is defined by

$$(\Delta G)_{:,j} := G_{:,j+1} - G_{:,j}, \quad j = 1, \dots, N-1. \quad (9)$$

B. Assumptions

Our theoretical analysis relies on the following assumptions.

Assumption 2. We impose the following conditions on the model, data, and optimization:

(A1) (Over-Parameterization) The model width satisfies

$$d_{\min} \geq C_1 \cdot \frac{N^2 \kappa_0^4}{\lambda_0^2} \cdot \log\left(\frac{N}{\delta}\right),$$

where $\kappa_0 := \max_i \|X^{(i)}\|_2$ is the maximum spectral norm of input sequences, $\lambda_0 > 0$ is a lower bound on the minimum eigenvalue of the neural tangent kernel (NTK) matrix [49], $\delta \in (0, 1)$ is the failure probability, and $C_1 > 0$ is a universal constant.

(A2) (Sequential Smoothness) The training samples are ordered such that consecutive samples satisfy

$$\|X^{(i+1)} - X^{(i)}\|_F \leq \frac{\beta}{\sqrt{N}}, \quad \forall i = 1, \dots, N-1,$$

for some smoothness constant $\beta > 0$.

(A3) (Initialization) The weight matrices are initialized independently as $(W_Q)_{ij}, (W_K)_{ij} \sim \mathcal{N}\left(0, \frac{2}{d_k}\right), (W_V)_{ij} \sim \mathcal{N}\left(0, \frac{2}{d_v}\right), (W_O)_{ij} \sim \mathcal{N}\left(0, \frac{2}{d_o}\right)$.

(A4) (Loss Regularity) The loss function $\ell(\cdot, y)$ is L_ℓ -Lipschitz continuous and has ρ_ℓ -Lipschitz continuous gradient for all y .

(A5) (Bounded Residual) The prediction residuals are uniformly bounded:

$$\|f(X^{(i)}; \theta) - y^{(i)}\|_2 \leq B_r, \quad \forall i = 1, \dots, N.$$

(A6) (NTK Eigenvalue Decay) The eigenvalues of the NTK matrix $\mathcal{K} \in \mathbb{R}^{N \times N}$ satisfy the polynomial decay condition:

$$\lambda_k(\mathcal{K}) \geq c_\lambda \cdot k^{-\alpha}, \quad k = 1, \dots, N,$$

for some constants $\alpha > 0$ and $c_\lambda > 0$.

Remark 4. These assumptions are standard in the neural network optimization literature:

- Assumption **(A1)** ensures that the network operates in the lazy training regime where NTK analysis applies [49]–[51];
- Assumption **(A2)** is natural for sequential data exhibiting temporal or spatial correlation;
- Assumption **(A3)** corresponds to He initialization [52] adapted for Transformer architectures;
- Assumptions **(A4)** and **(A5)** are mild regularity conditions satisfied by common loss functions such as cross-entropy and mean squared error;
- Assumption **(A6)** characterizes the spectral properties of the NTK, which has been studied extensively in [50], [53].

C. Main Result

Theorem 5 (Gradient Low-Rank Condition). *Under Assumption 2, let $\theta^{(0)}$ denote the random initialization. Then there exists a rank parameter*

$$r = \left\lceil \frac{2}{\alpha} \log N \right\rceil$$

such that, with probability at least $1 - \delta$ over the random initialization, the gradient matrix G satisfies

$$\|\Delta G\|_F < 0.1913\sqrt{N} \cdot \sigma_{r+1}(G), \quad (10)$$

provided that the model width satisfies

$$d_{\min} \geq \frac{C_2 \beta^2 B_r^2 \kappa_0^4 \log N}{0.0366 \cdot c_0^2}, \quad (11)$$

where $C_2 > 0$ is a universal constant and $c_0 > 0$ is defined in Lemma 7.

The proof of Theorem 5 relies on three key lemmas established below.

D. Supporting Lemmas

Lemma 4 (Softmax Lipschitz Property). *The softmax function $\sigma : \mathbb{R}^n \rightarrow \mathbb{R}^n$ defined by*

$$\sigma(z)_i = \frac{e^{z_i}}{\sum_{j=1}^n e^{z_j}}, \quad i = 1, \dots, n,$$

satisfies

$$\|\sigma(z) - \sigma(z')\|_2 \leq \|z - z'\|_2, \quad \forall z, z' \in \mathbb{R}^n.$$

Proof. The Jacobian of the softmax function is given by

$$J_\sigma(z) = \text{diag}(\sigma(z)) - \sigma(z)\sigma(z)^\top \in \mathbb{R}^{n \times n}.$$

For any vector $v \in \mathbb{R}^n$, we have:

$$\begin{aligned} \|J_\sigma(z)v\|_2^2 &= \|\text{diag}(\sigma(z))v - \sigma(z)(\sigma(z)^\top v)\|_2^2 \\ &= \sum_{i=1}^n \sigma(z)_i^2 v_i^2 - 2(\sigma(z)^\top v) \sum_{i=1}^n \sigma(z)_i^2 v_i + (\sigma(z)^\top v)^2 \\ &= \mathbb{E}_\sigma[v^2] - (\mathbb{E}_\sigma[v])^2 = \text{Var}_\sigma(v) \leq \mathbb{E}_\sigma[v^2] \leq \|v\|_2^2, \end{aligned}$$

where $\mathbb{E}_\sigma[\cdot]$ denotes expectation with respect to the probability distribution $\sigma(z)$. Thus $\|J_\sigma(z)\|_2 \leq 1$, and by the mean value theorem:

$$\|\sigma(z) - \sigma(z')\|_2 \leq \sup_{\xi \in [z, z']} \|J_\sigma(\xi)\|_2 \cdot \|z - z'\|_2 \leq \|z - z'\|_2.$$

Lemma 5 (Attention Perturbation Bound). *Under Assumption 2 **(A2)** and **(A3)**, for any two consecutive samples $X^{(i)}$ and $X^{(i+1)}$, the corresponding attention matrices satisfy*

$$\|A(X^{(i+1)}; \theta) - A(X^{(i)}; \theta)\|_F \leq \frac{C_A \kappa_0^2 \beta}{\sqrt{d_k N}},$$

with probability at least $1 - 2\exp(-d_k/8)$, where $C_A > 0$ is a universal constant.

Proof. For each sample $X^{(i)} \in \mathbb{R}^{n \times d}$, define the pre-softmax score matrix

$$S^{(i)} := \frac{X^{(i)} W_Q W_K^\top (X^{(i)})^\top}{\sqrt{d_k}} \in \mathbb{R}^{n \times n}.$$

Let $\Delta X := X^{(i+1)} - X^{(i)}$. Expanding the difference of the score matrices gives

$$S^{(i+1)} - S^{(i)} = \frac{1}{\sqrt{d_k}} \left(X^{(i+1)} W_Q W_K^\top (X^{(i+1)})^\top - X^{(i)} W_Q W_K^\top (X^{(i)})^\top \right).$$

Substituting $X^{(i+1)} = X^{(i)} + \Delta X$ and expanding all terms yields

$$S^{(i+1)} - S^{(i)} = \frac{1}{\sqrt{d_k}} \left(\Delta X W_Q W_K^\top (X^{(i)})^\top + X^{(i)} W_Q W_K^\top (\Delta X)^\top + \Delta X W_Q W_K^\top (\Delta X)^\top \right).$$

Taking Frobenius norms and using submultiplicativity together with $\|AB\|_F \leq \|A\|_F \|B\|_2$, we obtain

$$\|S^{(i+1)} - S^{(i)}\|_F \leq \frac{1}{\sqrt{d_k}} \left(\|\Delta X\|_F \|W_Q W_K^\top\|_2 \|X^{(i)}\|_F + \|X^{(i)}\|_F \|W_Q W_K^\top\|_2 \|\Delta X\|_F + \|\Delta X\|_F^2 \|W_Q W_K^\top\|_2 \right).$$

By Assumption **(A2)**, $\|X^{(i)}\|_F \leq \kappa_0$ and $\|\Delta X\|_F \leq \beta/\sqrt{N}$. Hence,

$$\|S^{(i+1)} - S^{(i)}\|_F \leq \frac{2\kappa_0 \|W_Q W_K^\top\|_2}{\sqrt{d_k}} \frac{\beta}{\sqrt{N}} + \frac{\|W_Q W_K^\top\|_2}{\sqrt{d_k}} \frac{\beta^2}{N}. \quad (12)$$

Under Assumption **(A3)**, standard spectral norm bounds for random matrices imply that with probability at least $1 - \exp(-d_k/8)$,

$$\|W_Q\|_2 \leq C_W \frac{\sqrt{d}}{\sqrt{d_k}}, \quad \|W_K\|_2 \leq C_W \frac{\sqrt{d}}{\sqrt{d_k}},$$

so that

$$\|W_Q W_K^\top\|_2 \leq \|W_Q\|_2 \|W_K\|_2 \leq C_W^2 \frac{d}{d_k}.$$

Substituting this bound into Eq. (12) and absorbing lower-order terms into the leading one gives

$$\|S^{(i+1)} - S^{(i)}\|_F \leq \frac{C_S \kappa_0 \beta}{\sqrt{d_k N}}$$

for some universal constant $C_S > 0$.

Finally, the attention matrix is obtained by applying the softmax row-wise:

$$A(X^{(i)})_{k,:} = \sigma(S_{k,:}^{(i)}).$$

Since the softmax mapping is 1-Lipschitz with respect to the Euclidean norm on each row, we have

$$\|A(X^{(i+1)}) - A(X^{(i)})\|_F \leq \|S^{(i+1)} - S^{(i)}\|_F.$$

Combining the bounds completes the proof. \square

Lemma 6 (Gradient Difference Upper Bound). *Under Assumption 2, the gradient matrix satisfies*

$$\|\Delta G\|_F \leq \frac{C_3 \beta B_r \kappa_0^2 \sqrt{N}}{\sqrt{d_{\min}}} \cdot \max_{1 \leq i \leq N} \|G_{:,i}\|_2,$$

where $C_3 > 0$ depends only on L_ℓ , ρ_ℓ , and architectural constants.

Proof. By the chain rule, the sample-wise gradient can be written as

$$G_{:,i} = \nabla_\theta f(X^{(i)}; \theta)^\top \nabla_f \ell(f(X^{(i)}), y^{(i)}) = J^{(i)} e^{(i)},$$

where $J^{(i)}$ is the Jacobian of the network output and $e^{(i)}$ is the loss gradient with respect to the output.

For two consecutive samples,

$$G_{:,i+1} - G_{:,i} = (J^{(i+1)} - J^{(i)}) e^{(i+1)} + J^{(i)} (e^{(i+1)} - e^{(i)}).$$

Taking Euclidean norms and using the triangle inequality,

$$\|G_{:,i+1} - G_{:,i}\|_2 \leq \|J^{(i+1)} - J^{(i)}\|_F \|e^{(i+1)}\|_2 + \|J^{(i)}\|_F \|e^{(i+1)} - e^{(i)}\|_2.$$

The perturbation bound on attention implies that

$$\|J^{(i+1)} - J^{(i)}\|_F \leq \frac{C_J \kappa_0^3 \beta}{\sqrt{d_{\min} N}}.$$

Moreover, Assumption **(A4)** gives $\|e^{(i)}\|_2 \leq L_\ell$, while the Lipschitz continuity of $\nabla_f \ell$ implies

$$\|e^{(i+1)} - e^{(i)}\|_2 \leq \rho_\ell \|f(X^{(i+1)}) - f(X^{(i)})\|_2 \leq \frac{C_f \rho_\ell \kappa_0^3 \beta}{\sqrt{d_{\min} N}}.$$

Using $\|J^{(i)}\|_F \leq C'_J \sqrt{m} \kappa_0$, we conclude that

$$\|G_{:,i+1} - G_{:,i}\|_2 \leq \frac{C\beta\kappa_0^2}{\sqrt{d_{\min}N}}$$

for a suitable constant C .

Summing the squared bounds over $i = 1, \dots, N-1$ yields

$$\|\Delta G\|_F^2 = \sum_{i=1}^{N-1} \|G_{:,i+1} - G_{:,i}\|_2^2 \leq \frac{C_3^2 \beta^2 B_r^2 \kappa_0^4 N}{d_{\min}} \max_i \|G_{:,i}\|_2^2,$$

which proves the claim. \square

Lemma 7 (Singular Value Lower Bound). *Under Assumption 2 (A1) and (A6), let*

$$r = \left\lceil \frac{2}{\alpha} \log N \right\rceil.$$

Then the gradient matrix satisfies

$$\sigma_{r+1}(G) \geq c_0 \frac{\|G\|_F}{\sqrt{r+1}},$$

where $c_0 > 0$ depends only on α , c_λ , and $\sigma_{\min}(E)/\|E\|_F$.

Proof. In the over-parameterized regime, the gradient matrix admits the approximation

$$G \approx \Phi^\top E,$$

where $\Phi_{:,i} = \nabla_\theta f(X^{(i)}; \theta^{(0)})$ and $E = [e^{(1)}, \dots, e^{(N)}]$.

The associated NTK matrix is $\mathcal{K} = \Phi^\top \Phi$. Its eigenvalues satisfy

$$\lambda_k(\mathcal{K}) = \sigma_k^2(\Phi).$$

By Assumption (A6),

$$\lambda_k(\mathcal{K}) \geq c_\lambda k^{-\alpha},$$

hence

$$\sigma_k(\Phi) \geq \sqrt{c_\lambda} k^{-\alpha/2}.$$

Using the inequality $\sigma_k(\Phi^\top E) \geq \sigma_k(\Phi) \sigma_{\min}(E)$, we obtain

$$\sigma_k(G) \geq \sqrt{c_\lambda} k^{-\alpha/2} \sigma_{\min}(E).$$

For $k = r+1$ with $r = \lceil \frac{2}{\alpha} \log N \rceil$, the decay condition ensures that $k^{-\alpha/2}$ is of order $(r+1)^{-1/2}$. Since $\|G\|_F^2 = \sum_k \sigma_k^2(G)$, comparison of the tail singular values with the Frobenius norm yields

$$\sigma_{r+1}(G) \geq c_0 \frac{\|G\|_F}{\sqrt{r+1}},$$

for a constant $c_0 > 0$ depending only on the spectral parameters. \square

E. Proof of Theorem 5

Proof of Theorem 5. We begin by combining the upper bound on the gradient perturbation from Lemma 6 with the lower bound on the singular value from Lemma 7.

Lemma 6 yields

$$\|\Delta G\|_F \leq \frac{C_3 \beta B_r \kappa_0^2 \sqrt{N}}{\sqrt{d_{\min}}} \cdot \max_{1 \leq i \leq N} \|G_{:,i}\|_2. \quad (13)$$

On the other hand, Lemma 7 ensures that

$$\sigma_{r+1}(G) \geq c_0 \frac{\|G\|_F}{\sqrt{r+1}}, \quad (14)$$

where $r = \lceil \frac{2}{\alpha} \log N \rceil$.

Dividing Eq. (13) by Eq. (14), we obtain

$$\frac{\|\Delta G\|_F}{\sigma_{r+1}(G)} \leq \frac{\frac{C_3 \beta B_r \kappa_0^2 \sqrt{N}}{\sqrt{d_{\min}}} \cdot \max_i \|G_{:,i}\|_2}{c_0 \frac{\|G\|_F}{\sqrt{r+1}}} = \frac{C_3 \beta B_r \kappa_0^2 \sqrt{N(r+1)}}{c_0 \sqrt{d_{\min}}} \cdot \frac{\max_i \|G_{:,i}\|_2}{\|G\|_F}.$$

Since $\|G\|_F^2 = \sum_{i=1}^N \|G_{:,i}\|_2^2$, we have the elementary bound

$$\max_{1 \leq i \leq N} \|G_{:,i}\|_2 \leq \|G\|_F.$$

Substituting this inequality into the previous display yields

$$\frac{\|\Delta G\|_F}{\sigma_{r+1}(G)} \leq \frac{C_3 \beta B_r \kappa_0^2 \sqrt{N(r+1)}}{c_0 \sqrt{d_{\min}}}. \quad (15)$$

We now determine a sufficient condition on the minimal width d_{\min} so that the desired inequality in Eq. (10) holds. It suffices to require

$$\frac{C_3 \beta B_r \kappa_0^2 \sqrt{N(r+1)}}{c_0 \sqrt{d_{\min}}} < 0.1913 \sqrt{N}.$$

Dividing both sides by \sqrt{N} and squaring the inequality gives

$$\frac{C_3^2 \beta^2 B_r^2 \kappa_0^4 (r+1)}{c_0^2 d_{\min}} < 0.1913^2.$$

Rearranging terms, we arrive at the sufficient width condition

$$d_{\min} > \frac{C_3^2 \beta^2 B_r^2 \kappa_0^4 (r+1)}{0.1913^2 c_0^2}. \quad (16)$$

Since $r = \lceil \frac{2}{\alpha} \log N \rceil$, we have $r+1 = O(\log N)$. Consequently, the right-hand side of Eq. (16) is of order

$$\frac{\beta^2 B_r^2 \kappa_0^4 \log N}{c_0^2}.$$

Therefore, a sufficient scaling is

$$d_{\min} = \Omega\left(\frac{\beta^2 B_r^2 \kappa_0^4 \log N}{c_0^2}\right),$$

which is ensured by Assumption **(A1)**.

Finally, we verify the probability statement. Lemma 5 holds with probability at least $1 - 2 \exp(-d_k/8)$ for each consecutive pair of samples. Taking a union bound over the $N-1$ pairs introduces a factor of N , and combining this with the concentration guarantee required for the NTK spectrum in Lemma 7, we conclude that the total failure probability is bounded by δ under the stated width condition.

This completes the proof. \square

Remark 6 (Interpretation). Theorem 5 establishes that the gradient matrix satisfies the required low-rank condition under:

- **Sufficient over-parameterization:** $d_{\min} = \tilde{\Omega}(\beta^2 B_r^2 \kappa_0^4)$;
- **Sequential smoothness:** consecutive samples have bounded variation;
- **Polynomial NTK decay:** eigenvalues decay as $k^{-\alpha}$ for some $\alpha > 0$.

Remark 7 (Connection to Low-Rank Adaptation). The condition Eq. (10) provides theoretical justification for methods such as LoRA [8], showing that gradient updates can be approximated by rank- r matrices with $r = O(\log N)$.

APPENDIX C EXPERIMENT DETAILS

A. Network Architecture

In this section, we describe the network architectures of the LLaMA (Large Language Model Meta AI) [29] and RoBERTa (Robustly Optimized BERT Approach) [36] models, which complement the experimental details provided in the main text. LLaMA is a family of foundational language models based on transformers [2]. For this paper, we adopt the LLaMA models from previous work [16], which use RMSNorm and SwiGLU activations [4], [29]. RoBERTa, on the other hand, is a variant of BERT (Bidirectional Encoder Representations from Transformers) [36], also built on the transformer architecture. Table VIII presents the architectural hyperparameters for the LLaMA and RoBERTa-base models, as well as the pre-training token amounts for LLaMA models across different sizes.

TABLE VIII
ARCHITECTURE HYPERPARAMETERS OF LLAMA FOR PRE-TRAINING. BATCH SIZE AND TRAINING DATA AMOUNT ARE SPECIFIED IN TOKENS.

Models	Params	Hidden	Intermediate	Heads	Layers	Iteration	Tokens
LLaMA	60M	512	1376	8	8	10K	1.3B
	130M	768	2048	12	12	20K	2.6B
	350M	1024	2736	16	24	60K	7.8B
	1B	2048	5461	24	32	100K	13.1B
	3B	2560	6848	32	32	120K	15.7B
RoBERTa	125M	768	3072	12	12	-	-

TABLE IX
HYPERPARAMETER lr , α , TRAINING GPUS, AND TRAINING TIME (HOURS) FOR DIFFERENT LLAMA MODELS. WE REPORT THE TRAINING TIME FOR ADAM WITH OUR GWT.

	60M	130M	350M	1B
Full-Adam	0.005, -	0.001, -	0.001, -	0.0005, -
GWT	0.01, 0.25	0.01, 0.25	0.01, 0.25	0.01, 0.25
GaLore	0.01, 0.25	0.01, 0.25	0.01, 0.25	0.01, 0.25
APOLLO	0.01, 1.0	0.01, 1.0	0.01, 1.0	0.01, 1.0
GPUs (RTX 3090)	4	4	16	32
Time	0.99h	4.03h	11.83	40.18h

B. Experiment Hyperparameters

In this section, we provide detailed information on the hyperparameters and experimental setup used in the experiments discussed in the main text. For the LLaMA pre-training tasks, we follow the experimental configuration used in previous work [7], which employs the default Adam hyperparameters ($\beta_1 = 0.9, \beta_2 = 0.999, \epsilon = 10^{-6}$), a maximum sequence length of 256 tokens, and gradient accumulation with a batch size of 512. Additionally, we apply a learning rate warm-up for the first 10% of the iterations and use a cosine annealing schedule with the initial learning rate.

For the GWT method, we perform hyperparameter tuning on the scale parameter α from the set $[0.1, 0.15, 0.2, 0.25]$, selecting the value that yields the best performance across all LLaMA pre-training tasks. We found that our method is not sensitive to scale, and setting α to 0.25 yields good results in most pretraining tasks, which is consistent with the hyperparameters used in previous work [7], [14]. For the baseline methods, we use their default hyperparameters: $\alpha = 0.25$ and $lr = 0.01$ for GaLore, and $lr = 0.001$ for Adam (0.0005 for Adam in LLaMA 1B and 3B). Consistent with prior work [7], we enable GWT and GaLore in the attention and MLP modules.

Finally, we summarize the hyperparameter α , the GPUs used (RTX 3090), and the training time (in hours) for our method required to reproduce the results shown of Table II in Table IX.

TABLE X
HYPERPARAMETER OF DIFFERENT MODELS ON THE MMLU BENCHMARK.

Hyperparameters	Adam	LoRA	GaLore	APOLLO	GWT
Rank r	-	8	8	8	-
Level l	-	-	-	-	8
Scale α	-	16	2	32	0.25
lr scheduler			Cosine		
Warmup steps			10%		
Epochs			3		
Batch size w. accumulation			32		
Where			All		
N-shots			5		
Cut-off length			2048		
lr (LLaMA3.2-3B)	1.0e-6	2.5e-5	1.0e-5	1.0e-6	1.0e-5
lr (Gemma3-4B)	1.0e-6	5.0e-6	2.5e-6	1.0e-6	1.0e-5
lr (Qwen2.5-7B)	-	2.5e-6	2.5e-6	1.0e-6	5.0e-5

For the MMLU fine-tuning tasks, we adopt the implementation from [54] for both the dataset identity and the Alpaca English [55] with a max training sample. For our GWT method, we use a fixed decomposition level of $l = 8$ across all evaluated models. This setting aligns the memory footprint with low-rank-based baselines that employ a rank of 8. The gradient scaling coefficient α is empirically set to $\alpha = \frac{1}{2^l}$. For other baselines, we follow the hyperparameter recommendations provided in

their original papers: $\alpha = 2$ for GaLore [7], $\alpha = 32$ for APOLLO [14], and $\alpha = 16$ ($2 \times r$) for LoRA [8]. In contrast to pre-training, we apply the memory-efficient fine-tuning technique to all linear layers during this task. We report the best accuracy obtained by sweeping the learning rate over the range [1.0e-6, 2.5e-6, 5.0e-6, 1.0e-5, 2.5e-5, 5.0e-5, 1.0e-4] for all the tested models fine-tuning. A summary of all used hyperparameters is provided in Table X.

C. Experiment Environments

We utilize the BF-16 format throughout all pre-training processes to optimize memory usage. All experiments were conducted on a setup of 1 to 8 server nodes, each equipped with four NVIDIA 3090 GPUs and an Intel(R) Xeon(R) Gold 6226R CPU @ 2.90GHz. The Python version used is 3.10, with PyTorch [56] version 2.3.1 for pre-training and 2.6.0 for MMLU fine-tuning. For the implementation of GWT, we leverage the PyTorch Wavelet Toolbox [57].

D. Memory and Throughput Estimates

In this section, we provide further clarification on the GPU memory usage results reported in the paper. First, Table I presents the theoretical memory consumption of various methods for comparison.

Compared to low-rank methods that reduce memory overhead by controlling the rank, our Gradient Wavelet Transform (GWT) method does not require additional storage for projection matrices. In practical experiments, GWT’s memory footprint is slightly **better** than these methods.

In actual training scenarios, GPU memory usage is influenced by multiple factors, including model size, batch size, optimizer states, PyTorch’s memory fragmentation management, and whether training is conducted on a single GPU or across multiple GPUs. To focus on core differences, we estimate GPU memory usage for the model weights and Adam optimizer states using bfloat16 precision. For example, the weights of the LLaMA 60M model occupy approximately 0.11 GB of GPU memory, while the Adam optimizer states require about 0.23 GB. Since GWT primarily targets reducing optimizer memory usage, the weight memory footprint under Adam with GWT remains unchanged at 0.12 GB.

As a representative example, the LLaMA-60M model contains approximately 58 million parameters. Using BF16 precision (2 bytes per parameter), this yields a model memory footprint of approximately 0.11 GB. The Adam optimizer maintains two auxiliary states—the first-order moment M and second-order moment V —each the same size as the model parameters, resulting in an additional 0.23 GB. The total memory usage with Adam is thus approximately 0.34 GB. For our GWT method, the computation formula depends on the number of parameters that use GWT and those that do not. Specifically, for LLaMA-60M, there are 25.3M parameters that use GWT to save memory, and the remaining 32.77M parameters are updated using Adam. In the case of using GWT with level $l = 2$, the optimizer states that the parameters are calculated as follows:

- The optimizer state for the GWT parameters:

$$25.3 \text{ M} \times 2 \text{ Bytes} \times 2/4 = 25.3 \text{ MBytes.}$$

- The optimizer state for the Adam parameters:

$$32.77 \text{ M} \times 2 \text{ Bytes} \times 2 = 131.08 \text{ MBytes.}$$

- The memory occupied by the model parameters:

$$116.14 \text{ MBytes.}$$

Therefore, the estimated training memory overhead with GWT-2 is

$$\begin{aligned} & 25.3 \text{ MBytes} + 131.08 \text{ MBytes} + 116.14 \text{ MBytes} \\ & = 272.52 \text{ MBytes} \approx 0.27 \text{ GBytes} \end{aligned}$$

Besides the memory estimate, we also report the training throughput as a complement to the training speed report. For example, we pre-train LLaMA 60M with a total batch size of 512 and a max sequence length of 256 in 10,000 iterations. This is equivalent to a total token size of $512 \times 256 = 131072 \approx 131\text{K}$ and a total of $131072 \times 10000 = 1310720000 \approx 1.3\text{B}$ tokens during the whole training process. In Tables XII and IX, we provide the training time and the number of GPUs used. Training LLaMA60M with our Haar-2 on four GPUs takes approximately 0.99 hours. Hence, we can compute the token throughput per GPU per second as $1310720000 / (0.99 \times 3600 \times 4) \approx 91.9\text{Ktokens/s}$

GWT level l . We investigate the effects of the GWT level hyperparameter l , with the corresponding validation perplexity curves shown in Figure 5. We found that the value of l has little impact on the final experimental results, and lower values of l are only slightly better than others. One question that arises from the experimental results is whether the approximation coefficients are not crucial when using wavelets to compress gradients in LLM training, but rather the detail coefficients. The main impact of l seems to be on memory usage and throughput. The throughput results and optimizer memory estimate for different GWT levels are summarized in Table XII, demonstrating the trade-off between memory efficiency and model performance. Higher wavelet levels improve memory usage, but this may come at the cost of slightly higher validation perplexity and slower training speed.

TABLE XI
MEMORY ESTIMATE OF WEIGHT PARAMETERS/OPTIMIZER STATES. * INDICATES RESULTS PUBLISHED IN PRIOR WORKS.

Methods	60M	130M	350M	1B
Full-Rank	0.11G/0.23G	0.26G/0.51G	0.68G/1.37G	2.60G/5.20G
MUON	0.11G/0.19G	0.26G/0.38G	0.68G/0.86G	2.60G/3.61G
GaLore-1/4	0.11G/0.17G	0.26G/0.32G	0.68G/0.70G	2.60G/2.16G
APOLLO-1/4	0.11G/0.17G	0.26G/0.32G	0.68G/0.70G	2.60G/2.16G
GWT-2	0.11G/0.16G	0.26G/0.29G	0.68G/0.56G	2.60G/1.81G
GaLore-1/8	0.11G/0.15G	0.26G/0.27G	0.68G/0.55G	2.60G/1.55G
APOLLO-1/8	0.11G/0.15G	0.26G/0.27G	0.68G/0.55G	2.60G/1.55G
GWT-3	0.11G/0.14G	0.26G/0.25G	0.68G/0.41G	2.60G/1.20G
Low-Rank*	0.08G/0.17G	0.18G/0.37G	0.36G/0.72G	1.19G/2.38G
LoRA*	0.20G/0.17G	0.44G/0.37G	1.04G/0.72G	3.79G/2.38G
ReLoRA*	0.20G/0.17G	0.44G/0.37G	1.04G/0.72G	3.79G/2.38G

TABLE XII
ESTIMATED OPTIMIZER MEMORY USAGE AND TOKEN THROUGHPUT (PER GPU) WITH DIFFERENT GWT LEVELS. HIGHER GWT LEVELS LEAD TO SLOWER TRAINING TOKEN THROUGHPUT BUT SMALLER MEMORY USAGE.

Methods	60M		130M		350M	
	Memory	Tokens/s	Memory	Tokens/s	Memory	Tokens/s
GWT-1	0.18G	95.8K	0.36G	46.0K	0.86G	12.7K
GWT-2	0.16G	91.9K	0.29G	45.1K	0.56G	12.1K
GWT-3	0.14G	90.1K	0.24G	44.8K	0.41G	11.5K
GWT-4	0.13G	84.2K	0.21G	43.8K	0.33G	10.8K
GWT-5	0.13G	83.5K	0.20G	41.5K	0.30G	9.25K

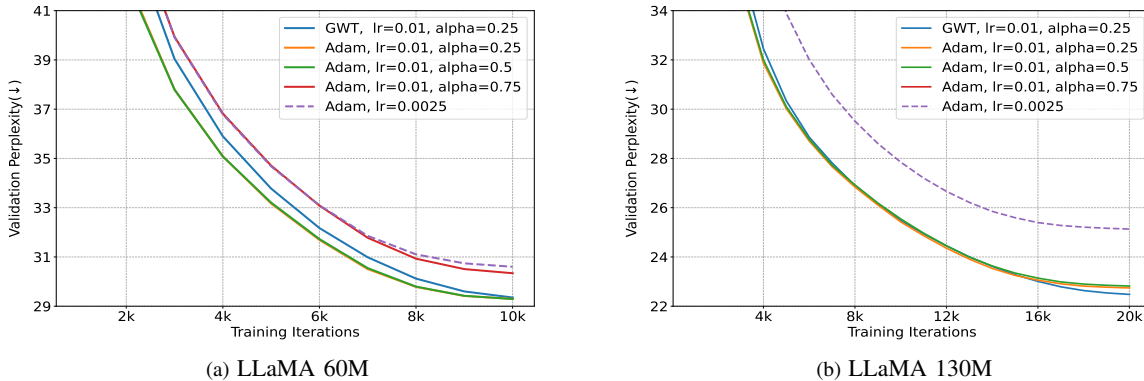


Fig. 7. **Applying module-wise learning rate to Adam optimizer.** We can observe that applying a module-wise split learning rate in Adam leads to better convergence speed and final results compared to using a uniform learning rate across all modules.

E. Adam with Module-wise Learning Rate

One key learning rate strategy employed in GWT is the assignment of different learning rates to distinct parameter modules. Specifically, the overall learning rate is partitioned such that the Attention and MLP modules are updated using a scaled learning rate of $lr \times \alpha$, while the rest of the model uses the base learning rate lr . This modular learning rate strategy is commonly adopted in memory-efficient training algorithms, including LoRA [8], GaLore [7], Fira [9], and APOLLO [14]. We incorporate this strategy into GWT as a standard configuration. The method of using different learning rates for different network modules in the Adam optimizer has been studied in related works [58], [59]. Here, we provide a supplement as an additional ablation experiment.

In this section, we first apply the same modular learning rate scheme to the Adam optimizer to examine whether it also benefits from this design, and to evaluate whether GWT can still match or surpass Adam’s performance, as demonstrated in the main text. Following standard practice in other memory-efficient methods, we use a learning rate of $lr \times \alpha$ for the Attention and MLP modules, while keeping lr for the remaining modules. To measure the benefit of this configuration, we compare it

with Adam using a unified learning rate of $2.5e-3$, selected from the range $[1e-3, 2.5e-3, 5e-3, 7.5e-3, 1e-2]$ based on best performance. The learning curves are shown in Figure 7.

Experimental results show that, under our setup, Adam significantly benefits from the modular learning rate strategy, achieving clearly better performance than with a single global learning rate. Even with this enhanced setting, GWT achieves a final validation perplexity (PPL) close to that of Full-Adam. This partly explains why many memory-efficient training methods can outperform full-rank Adam—the modular learning rate strategy plays a key role. It also suggests that Attention and MLP modules may require smaller learning rates than other parts of the model. These findings raise an important question: Do different modules in LLMs inherently demand distinct learning rates? And could explicitly integrating modular learning rate strategies into Adam lead to further gains?